A spike-timing-dependent plasticity rule for single, clustered and distributed dendritic spines

Authors

Sabrina Tazerart[1#], Diana E. Mitchell[1#], Soledad Miranda-Rottmann[1], and Roberto Araya[1*]

Affiliations

[1]Department of Neurosciences, Faculty of Medicine, University of Montreal

[#]These authors contributed equally to this work

*Corresponding author: Roberto Araya Ph.D. Assistant Professor, Department of Neurosciences, Faculty of Medicine, University of Montreal, C.P. 6128 Succursale Centre-Ville, Montreal, Quebec H3C 3J7, T: 514-343-7815, e-mail: roberto.araya@umontreal.ca

18 **SUMMARY**

19 The structural organization of excitatory inputs that supports spike-timing-dependent plasticity

20 (STDP) remains unknown. Here we performed a spine STDP protocol using two-photon

21 glutamate uncaging (pre) paired with postsynaptic spikes (post). We found that pre-post pairings

22 that trigger LTP (t-LTP) produce shrinkage of the activated spine neck and increase in synaptic

23 strength; and post-pre pairings that trigger LTD (t-LTD) decrease synaptic strength without

24 affecting spine shape. Furthermore, we tested whether this rule could be affected by the

25 activation of two clustered or distributed spines. We show that the induction of t-LTP in

26 clustered spines (<5 μm apart) enhances LTP through a mechanism dependent on spine calcium

27 accumulation and actin polymerization-dependent neck shrinkage, whereas t-LTD was disrupted

28 by the activation of clustered spines but recovered when separated by >40 μm. These results

29 indicate that synaptic cooperativity disrupts t-LTD and extends the temporal window for the

30 induction of t-LTP, leading to STDP only encompassing LTP.

31

INTRODUCTION

32

33   Dendritic spines, the main recipient of excitatory information in the brain [1], are tiny protrusions

34   with a small head (~1 μm in diameter and <1 fL volume) separated from the dendrite by a

35   slender neck. Spines can undergo structural remodeling that is tightly coupled with synaptic

36   function [1, 2, 3, 4], and are the preferential site for the induction of long-term potentiation (LTP) [4, 5,

37   6, 7] and long-term depression (LTD) [8], thought to be the underlying mechanisms for learning and

38   memory in the brain [9]. A variation of LTP and LTD has been described in pyramidal neurons

39   that involves the pairing of pre- and postsynaptic action potentials, known as spike-timing

40   dependent plasticity (STDP) [10, 11]. In this process, the timing between pre- and postsynaptic

41   action potentials modulates synaptic strength, triggering LTP or LTD [11]. The sign and magnitude

42   of the change in synaptic strength depends on the relative timing between spikes of two

43   connected neurons (the pre- and postsynaptic neuron [12]). The STDP learning rules and their

44   dependency on postsynaptic dendritic depolarization [13, 14], firing rate [13], and somatic distance of

45   excitatory inputs [14, 15, 16] have been extracted from studies using connected neuronal pairs or by

46   using extracellular stimulating electrodes, but the precise location and structural organization of

47   excitatory inputs capable of supporting STDP at its minimal functional unit – the dendritic spine

48   – are unknown.

49   Activity-dependent spine morphological changes (spine head [4], neck [2], or both [17]) have been

50   correlated with changes in synaptic strength in cortical pyramidal neurons by mechanisms

51   involving biochemical and electrical spine changes [1, 6]. Thus, here we asked what patterns of

52   activity and structural organization of excitatory synaptic inputs support the generation of t-LTP

53   and t-LTD, and which morphological, biophysical and molecular changes observed in dendritic

54   spines can account for the induction of t-LTP and t-LTD?

55   To induce synapse-specific STDP we performed a protocol whereby two-photon (2P) uncaging

56   of a caged glutamate (MNI-glutamate [3]) at a single spine – to mimic synaptic release – is

57   preceded or followed in time (STDP timing window [11]) by a backpropagating action potential

58   (bAP) to trigger t-LTP or t-LTD, respectively. Two-photon uncaging of a caged glutamate at a

59   single spine triggered excitatory postsynaptic potentials (uncaging(u)EPSP) that were recorded in

60   the soma of layer 5 (L5) pyramidal neurons before and after the induction of STDP, while the

61   morphology of the activated spine neck and head was monitored. To induce synapse-specific

62   STDP and monitor calcium levels in the activated spines and parent dendrites we performed a

63   protocol during which we perform nearly simultaneous 2P uncaging of glutamate and 2P calcium

64   imaging of the activated spines and nearby dendrites.

65   Here, we provide evidence showing that the induction of STDP in single or distributed spines

66   follows a bidirectional Hebbian STDP rule. Furthermore, we show that synaptic cooperativity,

67   induced by the co-activation of only two clustered spines, disrupt t-LTD (< 40 µm distance

68   between spines) and extend the temporal window for the induction of t-LTP (< 5 µm distance

69   between spines) via the generation of differential local calcium signals leading to an STDP rule

70   for clustered inputs only encompassing LTP.

4

71 **RESULTS**

72 **Induction of t-LTP in single dendritic spines**

73 To induce t-LTP, we used a repetitive spike-timing protocol (40 times, 0.5 Hz) in which 2P

74 uncaging of glutamate at a single spine was closely followed in time (+7 or +13 ms later, see

75 Methods section) by a bAP (Fig. 1A). We evaluated spine morphology and uEPSP amplitude for

76 40 min following STDP induction to establish the time course of STDP at individual synapses

77 (Fig. 1C.1 and D.1). In addition, the maximum uEPSP change and concomitant changes in spine

78 morphology observed in each experiment are shown (Fig. 1C.2 and D.2).

79 A repetitive pre-post pairing protocol of +13 ms reliably induced t-LTP (significant increase in

80 the uEPSP amplitude over time, $P < 0.001$, n = 7 experiments, from 6 neurons, from 6 mice, Fig.

81 1B.1 and C.1), and shortening of the activated spine neck within a few minutes ($P < 0.001$), with

82 no significant change in spine head volume (n = 7, Fig. 1B.2 and C.1). These results were also

83 consistent when we considered the maximum uEPSP change in amplitude from each experiment

84 and concomitant changes in spine morphology (uEPSP = 134.21 ± 3.29%, $P < 0.001$, n = 7; neck

85 length = 71.88 ± 10.66%, $P < 0.05$, n = 7; spine head volume = 98.11 ± 7.34%, $P = 0.81$, n = 7)

86 (Fig. 1C.2). We obtained similar results when we instead considered the average of all the values

87 obtained following t-LTP induction for uEPSP amplitude, neck length and head volume (Fig.

88 S1). This effect was specific to the activated spine (Fig. 1B.2), with neighbouring spines having

89 no appreciable changes in their neck length or head volume (neck length = 98.09 ± 5.06%, $P = $

90 0.71, n = 13; head volume = 103.01 ± 3.61%, $P = 0.42$, n = 14). Control experiments showed that

91 there was no significant change in uEPSP amplitude or spine morphology following the STDP

92 protocol when either action potentials or synaptic stimulation were applied in isolation, as well

93   as when we monitored the long-term stability of these parameters without any STDP protocol

94   (Fig. S2).

95   A pre-post pairing of + 7 ms showed a non-significant tendency for the induction of LTP

96   following t-LTP induction, and a non-significant tendency for the shrinkage of the activated

97   spine neck (n = 8 experiments, from 8 neurons, from 8 mice, Fig. 1D.1). When the maximum

98   change in uEPSP amplitude from each experiment and the concomitant changes in spine

99   morphology were analyzed, we saw no significant changes in uEPSP amplitude and spine

100   morphology (Fig. 1D.2, uEPSP = 112.27 ± 14.19%, P = 0.42, n = 8; neck length = 88.90 ±

101   5.89%, P = 0.10, n = 8; head volume = 97.81 ± 4.54%, P = 0.64, n = 8) (Fig. 2E). Similar results

102   were observed when we instead considered the average of all the values obtained following t-

103   LTP induction (+7 ms) for uEPSP amplitude, neck length and head volume (Fig. S1). Because

104   voltage has been shown to be an important factor in the induction of t-LTP and t-LTD, we

105   verified that the initial uEPSP amplitudes were not significantly different for pre-post pairing

106   protocols of +13 ms versus +7 ms (uEPSP: 0.62 ± 0.14 versus 0.53 ± 0.16 mV, P = 0.68; Fig.

107   S3).

108   These results indicate that for the pairing times tested, there is a preferred pre-post t-LTP pairing

109   time-window (+ 13 ms) at which activated spines in basal dendrites from L5 pyramidal neurons

110   undergo a significant increase in synaptic strength, and a concomitant neck shrinkage (Fig. 2E).

111

112   **Induction of t-LTD in single dendritic spines**

113   We then studied t-LTD in single spines by using a repetitive spike-timing protocol (40 times, 0.5

114   Hz) in which 2P uncaging of glutamate at a single spine was preceded in time (-15 or -23 ms) by

115   a bAP (post-pre protocol, Fig. 2A). When postsynaptic spikes preceded presynaptic firing by 15

116   ms (i.e., -15 ms), a significant reduction of the uEPSP amplitude occurred within a few minutes

117   following induction of t-LTD (n= 6 experiments, from 5 neurons and 5 mice, Fig. 2B.1 and C.1,

118    $P < 0.001$), with no significant changes in spine neck length or head dimension (Fig. 2B.2 and

119   C.1). Furthermore, when the maximum change in uEPSP amplitude after the induction of t-LTD

120   in single spines at pairings of -15 ms was analyzed (Fig. 2C.2) we also observed a significant

121   depression of uEPSP amplitude (uEPSP = 71.52 ± 7.07%, $P < 0.01$, n = 6), with no significant

122   changes in spine morphology (Fig. 2B.2 and C.2, neck length = 105.54 ± 9.85%, P = 0.62, n = 6;

123   head volume = 103.25 ± 3.02%, P = 0.33, n = 6). Interestingly, after the induction of t-LTD in

124   single spines when postsynaptic spikes preceded presynaptic firing by 23 ms (i.e., -23ms) there

125   were no significant changes in the amplitude of the uEPSPs or in the spine neck length and head

126   dimensions for the duration of the recordings (n= 7 experiments, from 7 neurons and 7 mice, Fig.

127   2D.1). These results were also consistent with analyses of the maximal uEPSP change in each

128   experiment and concomitant spine morphology (Fig. 2D.2: uEPSP = 82.09 ± 9.89%, P = 0.12, n

129   = 7; neck length = 84.15 ± 7.73%, P = 0.09, n = 7; head volume = 98.81 ± 5.57%, P = 0.84, n =

130   7). There was no significant difference between the initial uEPSP amplitude for post-pre pairing

131   protocols of -15 ms versus -23 ms (EPSP: 0.59 ± 0.07 versus 0.49 ± 0.08 mV, respectively, P =

132   0.42; Fig. S3). We obtained similar results when we instead considered the average of all the

133   values obtained following t-LTD induction in single spines for uEPSP amplitude, neck length

134   and head volume (Fig. S1). This indicates that for the pairing times tested, only a post-pre t-LTD

135   pairing time-window of -15 ms can effectively induce LTD in single dendritic spines in the basal

136   dendrites from L5 pyramidal neurons.

137   Taken together these results show that the induction of t-LTP and t-LTD in single spines follows

138   a Hebbian-STDP learning rule that is bidirectional, and favors presynaptic inputs that precede

139   postsynaptic spikes and depresses presynaptic inputs that are uncorrelated with postsynaptic

140   spikes at a very precise and narrow temporal window (+13 ms for the generation of t-LTP and -

141   15 ms for t-LTD, Fig. 2E-F). The single spine STDP rule we observed has a narrower post-pre

142   LTD induction pairing time window than previously observed in connected pairs of L2/3 [15, 18]

143   and L5 pyramidal neurons [13] – where the presynaptic control of t-LTD via an mGluR and/or

144   cannabinoid type 1 receptor-dependent mechanism [19, 20, 21, 22] could plausibly account for these

145   differences.

146

147   **Induction of t-LTP in clustered dendritic spines**

148   It has been suggested that STDP not only depends on spike timing and firing rate but also on

149   synaptic cooperativity and the amount of voltage generated at the postsynaptic site [13, 14].

150   Furthermore, it has been shown in mouse hippocampal CA1 pyramidal cells that the induction of

151   t-LTP in a single spine in low extracellular Mg^{2+} conditions can reduce the threshold for the

152   induction of plasticity of a neighboring spine (separated by < 10 µm) activated 90 seconds later [7].

153   However, a direct demonstration of synaptic cooperativity for synchronous, or nearly

154   synchronous synaptic inputs, in physiological extracellular Mg^{2+} conditions, and at the level of

155   single spines for the induction of STDP in the dendrites of pyramidal neurons has yet to be

156   obtained. Hence, we next directly tested if synaptic cooperativity, marked by the co-induction of

157   t-LTP in clustered dendritic spines from basal dendrites of L5 pyramidal neurons, and the local

158   spatio-temporal summation of inputs, can generate a local dendritic depolarization and local

159   calcium signals, which are high enough to disrupt the single spine STDP learning rule described

160   in Fig. 2E. To test this, a two spine STDP protocol (forty 2P uncaging pulses, pulse duration

161   2ms, 0.5Hz, see Methods section) was performed, whereby nearly simultaneous 2P uncaging of

162   caged glutamate in clustered (distance between spines < 5 μm) spines was followed in time by a

163   bAP to trigger t-LTP (Fig. 3A). With this protocol, we investigated whether activating clustered

164   spines extended the pre-post timing window capable of generating LTP by increasing the degree

165   of depolarization immediately before the postsynaptic spike at timings where plasticity was not

166   reliably generated. Specifically, we induced t-LTP in two clustered spines at pre-post timings of

167   +7 ms, and surprisingly found that this protocol was in fact capable of effectively and

168   significantly generating increases in uEPSP amplitude (Fig. 3B.1) and the concomitant shrinkage

169   of the activated spine neck, with no apparent changes in its spine head size (Fig. 3B.2). Pooled

170   data showed that significant increases in uEPSP amplitude and shrinkage of the spine neck of the

171   activated spines occurs only a few minutes post t-LTP induction and lasted for the duration of the

172   recordings (Fig. 3C, P < 0.01, n = 10 spines from 8 experiments, 6 neurons and 6 mice), with no

173   significant changes in the spine head size (Fig. 3C, n = 16 spines from 8 experiments, 6 neurons,

174   6 mice). Similar results were observed when we analyzed the maximal change in uEPSP

175   amplitude in each experiment and the concomitant spine neck length and head size of the two

176   clustered spines after induction of t-LTP at pairings of + 7 ms (Fig. 3H; uEPSP = 130.86 ±

177   8.18%, P < 0.01, n = 8; neck length = 73.22 ± 5.84%, P < 0.01, n = 10; head volume =102.00

178   ±2.58%, P = 0.45, n = 16). We obtained similar results when we instead considered the average

179   of all the values obtained following t-LTP induction in two clustered spines for uEPSP

180   amplitude, neck length and head volume (Fig. S1). In control experiments, no significant change

181   in uEPSP amplitude or spine morphology was observed when we monitored the long-term

182   stability of these parameters without any STDP protocol (Fig. S2B). These results indicate that

183   synaptic cooperativity of nearly simultaneous synaptic inputs – shown by the induction of t-LTP

184   in only two clustered spines (< 5 μm apart) – is sufficient to significantly trigger synaptic

9

185 potentiation and shrinkage of the activated spine necks at a pre-post timing that is otherwise

186 ineffective at generating significant morphological changes and synaptic potentiation when only

187 one spine is being activated (for comparison between one versus two clustered spines see Fig.

188 S4). Hence, the synaptic cooperativity of only two neighbouring synaptic inputs onto spines (< 5

189 μm apart) in the basal dendrites of L5 pyramidal neurons extends the pre-post timing window

190 that can trigger potentiation (Fig. 3H, and compare Fig. 3C with Fig. 1D.1).

191

192 **Induction of t-LTP in distributed dendritic spines**

193 To precisely study the effect of inter-spine distance of the nearly simultaneously activated spines

194 on synaptic cooperativity and the induction of t-LTP at pairings of +7 ms, we performed

195 experiments where the activated spines were further away (> 5 μm apart) from each other. When

196 we correlated 1) the inter-spine distance and the time at which the maximal uEPSP change was

197 observed for each experiment, or 2) the mean change - obtained when we analyzed the average

198 change in uEPSP from all the times tested for each experiment (Fig. S5A) - following t-LTP

199 induction, we found that as two activated spines were further away from each other, the less t-

200 LTP was induced (Fig. 3E-F, Fig. S5A). When the maximal uEPSP change per experiment was

201 analyzed, we observed that the induction of t-LTP decayed exponentially as a function of inter-

202 spine distance with a length constant (λ) of 5.7 μm (Fig. 3E). This value of λ was similar to that

203 obtained when we analyzed the average uEPSP change of all time points tested for each

204 experiment after t-LTP induction (Fig. S5A, P= 0.87, obtained when comparing the maximal

205 versus the average change in uEPSP used to calculate λ). Therefore we used this value as the

206 boundary between clustered (< 5 μm) and distributed (> 5 μm) spines for the induction of t-LTP

207 at pairings of + 7ms. Clustered spines were located in the same basal dendrite (n = 8/8 pairs),

208   while distributed spines were either in sister branches emanating from the same bifurcation point

209   (n = 7/13 pairs) or in the same basal dendrite (n = 6/13 pairs). By separating the data in this

210   manner, the t-LTP protocol (+ 7ms) in distributed spines (> 5 μm, Fig. 3D) failed to induce t-

211   LTP (Fig. 3F.1) or changes in spine head size and neck length at all the times tested post t-LTP

212   induction (Fig. 3G, n = 13 experiments, n = 26 spines, from 11 neurons and 7 mice). For

213   comparisons between the activation of two clustered versus two distributed spines with a pre-

214   post timing of + 7ms see Fig. S4. When we analyzed the maximum uEPSP change in amplitude

215   in each experiment and the concomitant changes in spine head volume and neck length in the

216   activated spines after t-LTP induction in two distributed spines, we also observed a complete loss

217   of t-LTP induction, with no changes in spine morphology (Fig. 3H; uEPSP = 92.52 ± 6.570%, P

218   = 0.28, n = 13 experiments; neck length = 94.76 ± 4.51%, P = 0.26, n = 20 spines; head volume

219   = 98.65 ± 2.41%, P = 0.58, n = 26 spines, from 13 experiments performed in 11 neurons from 7

220   mice). Similar results were obtained when we instead considered the average of all the values

221   obtained following t-LTP induction (+7ms) in distributed spines for uEPSP amplitude, neck

222   length and head volume (Fig. S1). In summary, this data shows that the induction of t-LTP in

223   nearly synchronously activated spines at pre-post timings of + 7 ms is disrupted when the two

224   activated spines were more than 5 μm apart in the basal dendrites of L5 pyramidal neurons.

225   These results uncover a two-spine activation crosstalk-spatial barrier of 5 μm for the induction of

226   t-LTP to occur at pre-post timings of + 7 ms.

227

228   **Molecular mechanisms responsible for the generation of t-LTP in dendritic spines**

229   The results led us to consider the possible mechanisms underlying the generation of t-LTP at the

230   level of single spines. Specifically, we asked why the induction of t-LTP in single and clustered

11

231   spines is associated with the shrinkage of the activated spine neck. We and others have reported

232   that the induction of LTP can trigger activity dependent changes in neck length [2, 17] and spine

233   head size [4, 6, 17], and that the amplitude of uEPSP recorded at the cell soma is inversely

234   proportional to the length of the activated spine neck [2, 23, 24]. However the mechanisms by which

235   the t-LTP-induced neck shrinkage is associated with synaptic plasticity remains unknown.

236   Numerical simulations show that the EPSP amplitude/neck length correlation can be explained

237   by variations in synaptic conductance, electrical attenuation through the neck, or a combination

238   of the two [2]. Nevertheless, solutions that rely exclusively on the passive electrical attenuation of

239   synaptic inputs through the spine neck assume very high (> 2 GOhm) neck resistance [2], which

240   are at odds with recent spine neck resistance estimations [25, 26]. These results suggest that the

241   control of AMPA receptor content in spines could contribute significantly to the observed t-LTP-

242   dependent changes in synaptic strength. To experimentally study the contribution of AMPA

243   receptors to these phenomena, we performed t-LTP experiments in two clustered spines from L5

244   pyramidal neurons recorded via patch pipettes loaded with intracellular solution containing 200

245   µM PEP1-TGL – a peptide that inhibits AMPA receptor incorporation to the postsynaptic

246   density (PSD) by blocking GluR1 C-terminus interaction with PDZ domains at the PSD [27] (Fig.

247   4A). PEP1-TGL incubation by itself did not trigger a run-down of uEPSP amplitude or changes

248   in spine morphology over time (Fig. S6A). Pooled data from experiments where a repetitive pre-

249   post pairing protocol of + 7 ms was used to activate clustered spines in the presence of PEP1-

250   TGL show that the peptide completely inhibited t-LTP for the duration of the experiment (Fig.

251   4B.1 and C.1), but had no effect on the t-LTP-induced shrinkage of the activated spine necks

252   (Fig. 4B.2 and C.1, $P < 0.001$, n = 6 spines, from 5 experiments, 5 neurons and 5 mice) or in

253   modifying spine head size (n = 10 spines, from 5 neurons and 5 mice, Fig. 4C.1). Furthermore,

254   when we analyzed the maximum change in uEPSP amplitude and the concomitant spine

255   morphology after the induction of t-LTP in the presence of PEP1-TGL, we also found an

256   inhibition of t-LTP, but no effect on the t-LTP-induced shrinkage of the spine neck (Fig. 4B.2-

257   C.2, uEPSP = 94.82 ± 14.82%, P = 0.74, n = 5 experiments, from 5 neurons and 5 mice; neck

258   length = 83.92 ± 5.35%, P < 0.05, n = 6; head volume = 100.08 ± 3.23%, P = 0.98, n = 10). We

259   obtained similar results when we instead considered the average of all the values obtained

260   following t-LTP induction in two clustered spines in the presence of PEP1-TGL for uEPSP

261   amplitude, neck length and head volume (Fig. S1). No significant difference was observed

262   between the initial uEPSP amplitude for pre-post pairing protocols of +7 ms with versus without

263   PEP1-TGL (uEPSP: 1.06 ± 0.2 versus 1.16 ± 0.28 mV, P = 0.81; Fig. S3). These results indicate

264   that GluR1 receptor incorporation into the PSD - via its interaction with PDZ domains - is

265   required for the induction of t-LTP in spines. However, the role of the spine neck shrinkage in

266   AMPA receptor incorporation into the PSD and ultimately on the induction of t-LTP remains

267   open.

268   Experimental and theoretical studies have indicated that lateral diffusion of AMPA receptors into

269   and out of the spine head can be restricted by the spine neck geometry [28, 29, 30, 31]. In particular,

270   lateral diffusion of AMPA receptors into and out of mushroom spines (long-necked spines) has

271   been shown to be significantly slower than that observed in stubby spines (small-necked spines)

272   [28] – which is supported by studies that show reduced diffusion of membrane proteins located in

273   spine necks [32]. In addition, quantitative models using realistic spine morphologies indicate that

274   decreasing the radius and increasing the spine neck length increases the retention of AMPA

275   receptors at the synapse [30], even when their interaction with scaffolding cytoskeletal proteins is

276   neglected [31]. Actin is highly enriched in the spine neck and head [33], and plays an important role

277   in anchoring AMPA receptors in the spine [34] and AMPA receptor trafficking [35], being

278   instrumental for synaptic transmission and plasticity [36, 37, 38]. Hence, to address the role that t-

279   LTP-induced neck shrinkage has on AMPA receptor lateral trafficking to the PSD, and the

280   generation of t-LTP in the activated spines we focused on actin dynamics. We used the actin

281   polymerization inhibitor latrunculin A (Lat-A) [34, 36, 38] (Fig. 4D), which did not trigger any run-

282   down of uEPSP amplitude or changes in spine morphology over time in the absence of STDP

283   induction (Fig. S6B), to test the potential role of actin dynamics on the spine induction of t-LTP,

284   and on the neck shrinkage and AMPA receptor incorporation into the PSD in the activated spines

285   (Fig. 4D). The induction of t-LTP at pre-post pairings of +7 ms in two clustered spines in the

286   presence of 100 nM Lat-A completely blocked the shrinkage of the activated spine necks and the

287   induction of t-LTP (Fig. 4E and F.1, n = 9 spines, from 8 neurons and 5 mice), inducing instead a

288   significant reduction in uEPSP amplitude over time (Fig. 4F.1, $P < 0.001$, n = 9 experiments,

289   from 8 neurons and 5 mice). These observations were also consistent with analyses of the

290   maximal change in uEPSP amplitude in each experiment and concomitant spine morphology

291   post t-LTP induction in the presence of Lat-A (Fig. 4F.2, uEPSP = $65.25 \pm 6.22\%$, $P < 0.001$, n =

292   9 experiments; neck length = $93.07 \pm 5.15\%$, $P = 0.2$, n = 14 spines; head volume = $103.6 \pm$

293   5.39%, $P = 0.51$, n = 16 spines).

294   We obtained similar results when we instead considered the average of all the values obtained

295   following t-LTP induction in two clustered spines in the presence of 100 nM Lat-A for uEPSP

296   amplitude, neck length and head volume (Fig. S1).

297   No significant difference was observed between initial uEPSP amplitudes for pre-post pairing

298   protocols of +7 ms with versus without Lat-A (uEPSP: 0.66 ± 0.1 versus 1.16 ± 0.28 mV, $P =$

299   0.11; Fig. S3). The lack of run-down of uEPSP amplitude over time in neurons treated with Lat-

300 A in the absence of STDP induction (Fig. S6B), but the significant depression in uEPSP after the

301 induction of t-LTP suggests that the induction of plasticity, and the rearrangement of actin

302 filaments de-stabilized AMPA receptors, leading to removal from the PSD.

303 In summary, these results show that actin polymerization is required for the t-LTP-dependent

304 neck shrinkage and the induction of plasticity. Our findings further suggest that the induction of

305 t-LTP occurs via a mechanism that involves a neck-shrinkage-dependent facilitated diffusion of

306 GluR1 subunits from the spine neck to the head, and subsequent incorporation into the PSD. We

307 hypothesize that a shorter and wider neck facilitates the transport of AMPA receptors into the

308 spine head (Fig. 4D), a mechanism that is required for the induction of t-LTP.

309

310 **Induction of t-LTD in clustered and distributed dendritic spines**

311 We then studied whether the induction t-LTD in single spines observed at pairings of -15 ms

312 could be affected by synaptic cooperativity. Our reasoning was based on two previous

313 observations which suggest that 1) t-LTP induction in the distal dendrites of L5 pyramidal

314 neurons (layer 3- L5 pyramidal neuron pairs) triggers LTD instead of LTP, and 2) that LTD can

315 be converted into LTP by increasing the local voltage [14]. We hypothesized that the induction of t-

316 LTD in single spines depends on the degree of local depolarization and hence, LTD can be

317 disrupted by the activation of neighboring spines. To test this, we performed repetitive spike-

318 timing protocol (40 times, 0.5 Hz) in which 2P uncaging of glutamate at two spines (separated by

319 up to 100 μm) was preceded in time (-15 ms) by a bAP (Fig. 5A.2 and Fig. S7A). Surprisingly,

320 we found that this t-LTD protocol failed to induce any change in uEPSP amplitude or spine head

321 volume with only a slight but significant reduction in spine neck length (Fig. S7A). When we

322 analyzed the maximum uEPSP change in amplitude in each experiment and the concomitant

15

323   morphological alterations in the activated spines after t-LTD induction, we observed a complete

324   inhibition in the induction of t-LTD, and no change in spine morphology (Fig. S7B; uEPSP =

325   93.22 ± 6.29%, P = 0.30, n = 17 experiments from 14 neurons and 14 mice; neck length = 88.56

326   ± 5.69%, P = 0.06, n = 23 spines; head volume = 102.41 ± 6.10%, P = 0.69, n = 34 spines). To

327   more precisely characterize the effect of activating two spines on the induction of t-LTD, we

328   correlated the inter-spine distance and either 1) the maximum uEPSP change from each

329   experiment or 2) the mean uEPSP change of all the times tested from each experiment following

330   STDP induction (see Methods). We found that as the two activated spines were further away

331   from each other, the more t-LTD was recovered (Fig. 5D, each data point corresponds to the time

332   at which the maximal change in uEPSP was observed after t-LTD induction). Specifically, the

333   uEPSP change decayed exponentially as a function of inter-spine distance with a length constant

334   (λ) of 43.5 μm. This value of λ was similar to that obtained when we analyzed the average

335   uEPSP change of all time points tested for each experiment after t-LTD induction (Fig. S5B, P=

336   0.8, obtained by comparing the maximal versus the average change in uEPSP used to calculate

337   λ).Therefore, we used this value as a boundary between clustered (< 40 μm) and distributed (>

338   40 μm) spines. Using this classification, clustered spines were located in the same dendrite (n =

339   11/12 pairs) or in sister branches emanating from the same bifurcation point (n = 1/12 pairs),

340   while distributed spines were always located on separate dendrites (n = 5/5 pairs). When we

341   separated our data in this manner, the t-LTD protocol in two clustered spines (Fig. 5A) failed to

342   induce t-LTD (Fig. 5B.1) or changes in spine head size at all the times tested post t-LTD

343   induction (Fig. 5B.2 and C, n = 12 experiments, n = 24 spines, from 11 neurons and 11 mice),

344   with only a slight but significant induction of shrinkage of the spine neck at some time points

345   (Fig. 5C, P < 0.05, n = 19 spines, from 11 neurons and 11 mice). For comparison between the

346   activation of one versus two clustered spines with a post-pre timing of -15 ms see Figure S8.

347   When we analyzed the maximum uEPSP change in amplitude in each experiment and the

348   concomitant morphological alterations in the activated spines after t-LTD induction in two

349   clustered spines, we also observed a complete inhibition in the induction of LTD, a slight but

350   significant reduction in spine neck length, and no changes in spine head size (Fig. 5G; uEPSP =

351   101.70 ± 7.02%, P = 0.81, n = 12 experiments; neck length = 85.28 ± 5.96%, P < 0.05, n = 19

352   spines; head volume = 102.98 ± 8.86%, P = 0.73, n = 24 spines, from 12 experiments performed

353   in 11 neurons from 11 mice). We obtained similar results when we instead considered the

354   average of all the values obtained following t-LTD induction in clustered spines for uEPSP

355   amplitude, neck length and head volume (Fig. S1). These results were surprising since not only

356   did we not observe t-LTD in clustered spines, but we also observed significant neck shrinkage

357   with no LTP (see Fig. 1 and 3). To account for this observation, we explored if there was a

358   correlation between the induction of plasticity in these experiments and both the shrinkage of the

359   spine neck and the distance between the activated clustered spines – since the local voltage, and

360   hence the induction of plasticity, could be affected by the distance between the activated

361   clustered spines. Indeed, we found that the distance between the activated spines under these

362   experimental conditions (t-LTD induction protocol in clustered spines) is correlated with the

363   induction of plasticity and the shrinkage of the activated spine necks (Equation 1 in Methods; P

364   < 0.01; Fig. S7D). This analysis suggests that during t-LTD induction the structural arrangement

365   of clustered spines (< 40 µm) determines the sign and magnitude of the change in synaptic

366   strength and concomitant neck shrinkage.

367   We next investigated the mechanisms underlying the disruption of t-LTD by activating spines

368   separated by increasingly larger distances (Fig. 5A.2). Interestingly, the induction of t-LTD in

369   spines separated by more than 40 μm (distributed spines) was capable of recovering the

370   generation of LTD (Fig. 5D-E). Pooled data from all experiments demonstrate that the activation

371   of distributed spines reliably induces t-LTD (Fig. 5F, significant reduction in uEPSP amplitude,

372   $P < 0.01$, n = 5 experiments from 5 neurons and 5 mice), without triggering changes in neck

373   length or spine head size (Fig. 5E and F). When we analyzed the maximal change in uEPSP

374   amplitude in each experiment and concomitant spine morphological changes, we saw a

375   significant induction of t-LTD and no change in spine morphology (Fig. 5G, uEPSP = 72.86 ±

376   8.08%, $P < 0.05$, n = 5 experiments, neck length = 97.85 ± 15.47%, $P = 0.89$, n = 6 spines; head

377   volume = 101.06 ± 4.59%, $P = 0.82$, n = 10 spines) as what was found in experiments where t-

378   LTD was generated at pairing times of -15 ms in single dendritic spines (Fig. 2B-C). We

379   obtained similar results when we instead considered the average of all the values obtained

380   following t-LTD induction in distributed spines for uEPSP amplitude, neck length and head

381   volume (Fig. S1). No significant difference was observed between the initial uEPSP amplitude

382   for clustered versus distributed spines activated with post-pre pairings of -15 ms (EPSP: 1.06 ±

383   0.13 versus 1.31 ± 0.19 mV, $P = 0.25$; Fig. S3). For comparison between the activation of

384   clustered versus distributed spines after post-pre pairings of -15 ms, see Figure S8.

385   In summary, this data shows that the induction of t-LTD at pairing times of -15 ms was disrupted

386   when only two clustered spines (< 40 μm apart) were nearly simultaneously activated in the

387   basal dendrites of L5 pyramidal neurons, but could be recovered if the activated spines are

388   distributed (> 40 μm) in the dendritic tree.

389

390   **Spine calcium transients during the induction of t-LTP and t-LTD in single and clustered**

391   **dendritic spines**

392   Calcium is critical for the induction of synaptic plasticity [39, 40, 41, 42, 43], and high or low local

393   concentration difference in dendrites and spines are thought to be associated with gating LTP or

394   LTD, respectively [44, 45, 46]. Therefore, to investigate the different mechanisms – with respect to

395   local calcium accumulations – underlying the induction of t-LTP and t-LTD in single versus two

396   clustered spines, we performed 2P calcium imaging in a region of interest (ROI) of the activated

397   spines and their parent dendrites during STDP induction protocols throughout each of the 40 pre-

398   post or post-pre repetitions (see Methods).   The "before" images correspond to the calcium

399   signals observed in the ROI right before the pairing in each repetition – uncovering the lack or

400   presence of local calcium accumulation during the 40 pairing repetitions.   The "after" images

401   correspond to the calcium signals observed in the ROI right after the pairing in each repetition –

402   uncovering a proxy for the amplitude and local calcium accumulation during the 40 pairing

403   repetitions.

404   To dissect potential differences in local calcium signals and accumulation that can account for

405   the presence or absence of t-LTP and t-LTD induction in clustered versus distributed spines, we

406   imaged 2P calcium activity during five different STDP induction protocols: (1) pre-post pairing

407   of +7 ms in one spine; (2) pre-post pairing of +7 ms in two clustered spines; (3) pre-post pairing

408   of +13ms in one spine; (4) post-pre pairing of -15 ms in one spine; (5) post-pre pairing of -15 ms

409   in two clustered spines.

410   During the pre-post (+7 ms) pairing protocol in single spines we found that, across the 40

411   repetitions, there was little to no calcium accumulation in the spine or dendrite (Fig. 6A and left

412   panels in Fig. 6B, n = 7 experiments, from 6 neurons, and 4 mice). As expected, there was,

413   however, a significant increase in calcium immediately following the stimulation (left panels in

414   Fig. 6D) that due to the lack of accumulation throughout the 40 repetitions, did not build up a

415   local calcium signal in the activated dendrites and spines. In contrast, when we applied the exact

416   same pairing protocol (pre-post + 7ms) in two clustered spines, there was a striking calcium

417   accumulation in both the activated spines and dendrite that was evident when we analyzed the

418   images taken before (Fig. 6C and middle panels in Fig. 6B) and after stimulation (middle panels

419   in Fig. 6D, n = 6 experiments, from 4 neurons, and 4 mice). Thus, activating just one additional

420   spine using the same pairing protocol alters the calcium dynamics (compare black and green

421   traces in right panels of Fig. 6B and D), possibly through a mechanism that is incapable of

422   extruding calcium increases in spines in between pre-post repetitions, leading to its build up in

423   spines and parent dendrites, which ultimately guide the induction of plasticity.

424   Since the activation of a single spine with a repetitive pre-post pairing protocol of +13 ms

425   reliably induced t-LTP (Fig. 1B-C), we performed experiments to measure the calcium signals in

426   the activated spine and parent dendrite during the pre-post (+13 ms) pairing protocol. We found

427   that, across the 40 repetitions, there was a significant calcium accumulation in both the activated

428   spine and dendrite that was evident when we analyzed the images taken before (Fig. 7A and B)

429   and after stimulation (Fig. 7A and C).

430   In summary, the induction of t-LTP in a single spine at a pre-post pairing protocol of +13 ms

431   (Fig. 7) and in clustered spines at a pairing time of +7ms (which is otherwise ineffective in

432   triggering t-LTP if only one spine is being activated) (Fig. 6) are correlated with an accumulation

433   of calcium in spines and parent dendrites, likely being responsible for the induction of t-LTP.

434   Next, we performed the same experiments with a post-pre (-15 ms) pairing protocol in both

435   single and clustered spines. In single spines, we observed moderate calcium increases (Fig. 8A, n

436   = 5 experiments, from 4 neurons, and 4 mice) that were observed when we analyzed images

437   taken before (left panels in Fig. 8B) and after the post-pre stimulation (left panels in Fig. 8D).

20

438   Surprisingly, we found similar results to those observed with single spine t-LTD induction

439   protocols, when we applied the same pairing protocol in two clustered spines (Fig. 8C, n = 6

440   experiments, from 4 neurons, and 3 mice) before (middle panels in Fig. 8B) or after the induction

441   protocol (middle panels in Fig. 8D), even though no plasticity is induced in this condition. As

442   suggested by previous studies [47], we hypothesize that the range of spine calcium levels required

443   for the induction of t-LTD is relatively narrow, and that the resolution with our current

444   experimental set-up is not sufficient to tease apart significantly different calcium dynamics in

445   one versus two clustered spines during a post-pre pairing protocol of -15 ms. Moreover, models

446   of STDP provide evidence that, in addition to overall calcium levels, the detailed time course of

447   calcium levels in the postsynaptic cell during a pairing protocol also guide the induction of

448   plasticity [48]. Nonetheless, these results suggest that the induction of t-LTD does not require

449   significant calcium accumulations during the 40 repetitions, and most likely depends on the

450   amplitude of calcium signals right after the stimulation.

451   **DISCUSSION**

452   We uncovered the STDP rules for single, clustered and distributed dendritic spines in the basal

453   dendrites of L5 pyramidal neurons. Our results show that the induction of STDP in single spines

454   follows a classical Hebbian STDP learning rule that is bidirectional, in which presynaptic input

455   leading postsynaptic spikes generates t-LTP and postsynaptic spikes preceding presynaptic

456   activation of single dendritic spines results in t-LTD. Furthermore, we found that the induction of

457   t-LTP triggers the shrinkage of the activated spine neck, without any significant changes in the

458   spine head size, building upon our previous findings of the activity-dependent shrinkage of the

459   spine neck [2]. Our results indicate that the induction of t-LTP requires 1) the incorporation of new

460   GluR-1 receptors with PDZ-domain containing proteins in the PSD and, 2) an actin

461   polymerization-dependent neck shrinkage of the activated spine neck (Fig. 4). We showed that

462   the induction of t-LTP triggers actin-dependent neck shrinkage, which is likely required for the

463   lateral diffusion of GluR-1 receptors from the spine neck to the spine head, and its incorporation

464   to the PSD – generating plasticity. In support of this spine mechanism of LTP induction is a

465   recent report showing that AMPA receptor surface diffusion is fundamental for the induction of

466   hippocampal LTP and contextual learning [49]. In addition, we found that the induction of t-LTD

467   was not accompanied with spine neck or head changes, which is at odds with previous findings

468   suggesting structural changes in spine head volume during the induction of LTP or LTD [4, 8, 50].

469   The discrepancy between our results and those observed previously after the induction of t-LTP

470   (head enlargement [7, 50]), LTP [4], or LTD (head shrinkage, [8]) using glutamate uncaging are likely

471   explained by methodological differences. While our data was obtained using ACSF with

472   physiological concentrations of magnesium and calcium, those from other reports were done in

473   low or a magnesium-free ACSF [4, 8], low calcium extracellular solution for the induction of LTD

22

474   [8], or in a magnesium-free ACSF and an intracellular solution containing 5 µM actin that was

475   required for the t-LTP-mediated spine head enlargements [50].

476   Nonetheless, it has been shown in vivo that a spike-timing protocol triggers receptive field

477   plasticity in layer 2/3 pyramidal neurons is correlated with spine head volume changes

478   (enlargement and shrinkage) observed after 1.5-2 hours [51]. Taken together, these data, and

479   previous observations [2], suggest that there is a new form of structural spine plasticity during t-

480   LTP that involves rapid neck shrinkage without head volume enlargements. In addition, we show

481   that the induction of t-LTD does not require structural spine changes. Although spines have the

482   machinery and do undergo structural head changes, we propose that our results represent a stage

483   during memory formation that occurs before structural head volume changes, a process likely

484   linked with memory consolidation. Importantly, our data suggest that during STDP, the use of

485   spine volume changes as the sole proxy for LTP or LTD [51] is not a complete representation of

486   plasticity in spines from dendrites in cortical pyramidal neurons.

487   We then explored the functional consequences of synaptic cooperativity of nearly simultaneous

488   excitatory inputs on STDP. Our results show that the induction of t-LTP in two clustered spines -

489   separated by less than 5 µm - is sufficient to induce LTP and shrinkage of the activated spine

490   necks at a pre-post timing (+ 7ms) that is otherwise ineffective at triggering significant

491   morphological changes and synaptic potentiation when only one spine is being activated. To

492   uncover the distance between the nearly simultaneously activated spines capable of supporting

493   synaptic cooperativity and the induction of t-LTP, we varied the distance of the activated spines.

494   Our results show that the induction of t-LTP is suppressed when spines are separated by more

495   than 5 µm apart (Fig. 3 and Fig. S5A), with an effective length constant (λ), that represents the

496   length at which the electrotonic potential decays to a value of 37% of that at the point of origin,

23

497   of 5.7 µm These results show that the nearly simultaneous activation of clustered spines, less

498   than < 5 µm apart, can extends the pre-post timing window that can trigger potentiation. This

499   data, together with results showing that the induction of t-LTP in one spine can change the

500   threshold for the induction of plasticity in a spine located at less than 10 µm away and activated

501   90 seconds later [7], indicate that there is a spatially restricted dendritic compartment that is

502   required for spine crosstalk and the broadening of the STDP timing required for triggering t-LTP

503   (Fig. 9).

504   On the other hand, the induction of t-LTD in two clustered spines disrupts the generation of LTD

505   leading to a STDP learning rule that is incapable of supporting LTD, but only encompasses LTP

506   (Fig. 9). We next investigated the dendritic mechanisms responsible for the disruption of t-LTD,

507   and found that the induction of t-LTD is recovered when the activated spines are separated by

508   more than 40 µm (Fig. 5, Fig. 9 and Fig. S5B). Interestingly, the effective length constant (λ) in

509   the basal dendrites of L5 pyramidal neurons has been reported to be 50 µm [52]. This value of λ

510   supports the idea that significant voltage attenuations – capable of recovering LTD – can be

511   expected when the t-LTD induction protocol is triggered in spines that are separated by more

512   than 40 µm in the basal dendrites of L5 pyramidal neurons (Fig. 5D-G). However, we cannot

513   discard that other mechanisms, such as the diffusion of active molecules [5], could contribute to

514   the switch from t-LTD to no-LTD induction observed in distributed/single spines and clustered

515   spines, respectively. These results are in discrepancy with observations showing that in

516   connected pairs of L5-L5 pyramidal cells, t-LTD is reliably generated after post-pre pairing

517   protocols [13]. A likely explanation for this apparent controversy is that the synaptic inputs from

518   one L5 pyramidal neuron to another are distributed [53]. Importantly, clustered and distributed

519   excitatory inputs have been described in the dendrites of pyramidal neurons both *in vitro* and *in*

520   *vivo* [1, 54, 55, 56]. Our results clearly show the functional importance that the structural and temporal

521   organization of excitatory synaptic inputs have on the induction of t-LTP and t-LTD, and how

522   just two clustered excitatory synaptic inputs are capable of altering the STDP learning rule in the

523   basal dendrites of L5 pyramidal neurons (Fig. 9).

524   How the synaptic activation of just one extra clustered spine is capable of (1) inducing t-LTP at a

525   pre-post timing that is otherwise ineffective in inducing potentiation and (2) disrupting the

526   induction of t-LTD? To explore the mechanisms that may be responsible for these observations

527   we imaged local calcium signals in the activated spines and parent dendrites before and after

528   each of the 40 pairings performed during t-LTP and t-LTD induction protocols. Our reasoning

529   for performing these experiments was based on findings that different levels of depolarization

530   gate local calcium signals, which depending on its magnitude and kinetics, can generate LTP

531   (high calcium) or LTD induction (sustained but moderate calcium signals) [10, 44, 57]. In addition,

532   calcium-based modeling studies of STDP have shown that different calcium dynamics mediate

533   the induction of t-LTP versus t-LTD [47, 48]. Specifically, the calcium control hypothesis indicates

534   that large levels of calcium (above a plasticity threshold, Θ_p) are thought to lead to t-LTP

535   whereas more moderate, prolonged levels (between the depression threshold, Θ_{dSTART}, and

536   Θ_{dSTOP})) give rise to t-LTD and a mid-level range in which t-LTD does not occur (below

537   Θ_{dSTART}) [48, 58, 59]. A major assumption of these models is infinite time constants for synaptic

538   variables at resting calcium levels so that the synaptic changes do not to decay after the

539   presentation of the stimulus [47] - a significant constraint for the stabilization of synaptic changes.

540   A potential solution to this problem is the degree of local calcium accumulation observed in the

541   activated spines throughout the t-LTP or t-LTD induction protocol. In fact, these models are

542   consistent, fundamentally, with our results which show that a pre-post pairing of +7 ms protocol

25

543 in two clustered spines, and a pre-post pairing of +13 ms protocol in a single spine gives rise to t-

544 LTP accompanied by a substantial increase in the intracellular calcium levels following each

545 pairing repetition, and a significant accumulation of local calcium levels throughout the

546 induction protocol – likely mediated by the inability to efficiently extrude the local calcium

547 signals in between each pre-post pairing at this induction frequency (Fig. 6 and 7). We propose

548 that the local spine calcium accumulation we observe provides a new and key variable for the

549 induction of plasticity, which reduces the constraints imposed by calcium-base models for the

550 stabilization of synaptic changes [47, 48, 58, 59].

551 These changes in local spine and dendritic calcium signals observed when clustered spines are

552 activated at pairings of + 7ms (Fig. 6) or in a single spine activated at pairings of + 13ms (Fig. 7)

553 suggest that perhaps Θ_p can be reached only with ~ 10-20 pre-post pairings (~20-40 seconds). In

554 contrast a pairing protocol of + 7ms in one spine induces no plasticity, and calcium levels that

555 are effectively extruded in between pairings leading to no calcium accumulation during the

556 induction protocol (reaching levels below Θ_p and Θ_{dSTART}). These results suggest that it is not

557 only the amplitude of the local calcium signals after each pairing, but also the local calcium

558 accumulation during the induction protocol (40 pairings, ~80 seconds) in spines and dendrites

559 that are required to reach Θ_p for the induction of t-LTP in clustered spines. As mentioned before,

560 recently it has been demonstrated in vivo that spike timing-induced receptive field plasticity,

561 with millisecond time delays between visual stimulus (pre) and optogenetic stimulation in layer

562 2/3 pyramidal neurons (post), is correlated with increases in synaptic strength [51]. These results

563 together with evidence from other in vivo studies showing that layer 5 pyramidal neurons can

564 spike up to frequencies of 20 Hz during movement [60], suggest that our pairing protocol, and

26

565   findings, are likely present under certain in vivo conditions and are relevant for plasticity of

566   networks and ultimately behaviour.

567   Our results further show that a post-pre protocol of -15 ms in a single spine induces t-LTD and

568   moderate intracellular calcium signals in spines and parent dendrites after each pairing, without

569   an evident increase in local calcium accumulation. These results possibly reflect that the calcium

570   signal generated during the induction protocol passed Θ_{dSTART} and remained for several seconds

571   in this permissive calcium concentration window – between Θ_{dSTART} and Θ_{dSTOP} – generating

572   LTD. Activating two clustered spines with the same protocol, however, does not induce

573   plasticity and gives rise to an apparent smaller initial calcium accumulation than that observed

574   with the activation of a single spine but with a slow build-up of calcium. These results possibly

575   reflect that the spine calcium levels crossed Θ_{dSTART} only after > 20 repetitions and then crossed

576   Θ_{dSTOP} and Θ_{pSTART} after a few (<10) repetitions reaching slightly higher local calcium levels.

577   Further experiments to prove this calcium control hypothesis of t-LTD induction, with better

578   temporal detection tools are needed.

579   These findings presented here are quite remarkable since stimulating just one additional spine

580   during a STDP protocol can alter the calcium dynamics and the induction of t-LTP and t-LTD.

581   To our knowledge, this is the first demonstration of the functional relevance that the structural

582   organization and nearly simultaneous subthreshold activation of only a few clustered inputs in

583   the dendrites of pyramidal neurons have on plasticity. We propose the term *micro clusters* to

584   describe this structural and functional modality of synaptic connectivity. In fact, the relevance of

585   synaptic *micro clusters* on the input/output properties of pyramidal neurons is also supported by

586   three dimensional electron microscopy and neuronal reconstruction studies that have shown the

587   presence of postsynaptic innervation of the same axon spaced at less than 10 µm in the basal

27

588 dendrites of L2/3 pyramidal neurons from the medial entorhinal cortex [54], L5 pyramidal neurons

589 from somatosensory cortex [55] and in the distal apical tuft dendrites in stratum lacunosum-

590 moleculare of hippocampal CA1 pyramidal neurons [56]. In addition to having spines innervated

591 by the same axon, it is likely that functional synaptic *micro clusters* can be gated by the

592 convergence of different axons, which could increase the computational power of cortical

593 circuits through a multi-neuronal control of synaptic cooperativity and ultimately the

594 implemented STDP learning rule. Furthermore, it has been shown that orientation selectivity in

595 visual cortex is correlated with the degree of spatial synaptic clustering of co-tuned synaptic

596 inputs within the dendritic field [61], and that functional clusters of dendritic spines separated by

597 less than 10 μm share similar spatial receptive field properties, spontaneous and sensory-driven

598 activity [62]. Interestingly, is has been recently shown in the mouse visual cortex that a single axon

599 can contact clustered synapses in the postsynaptic neuron, but that local clustering is not

600 favoured over widespread spacing of synaptic inputs [63]. In addition, recently it has been

601 demonstrated in L2/3 pyramidal neurons from mouse primary visual cortex that synaptic *micro*

602 *clusters* reflects the interaction of functionally similar inputs - with similar orientation preference

603 - from different sources – callosal and non-callosal inputs [64], providing functional and anatomical

604 data for the presence of multi-neuronal control of synaptic cooperativity in a short dendritic

605 segment. Moreover, it has been shown that coactive neighboring synapses drive the maturation

606 of cluster synapses in CA1 pyramidal neurons [65], suggesting that *micro clusters* also play an

607 important role in the development and shaping of network connectivity. Taken together these

608 reported findings and our data suggest that the functional specificity and structural arrangement

609 of synaptic inputs, distributed or forming *micro clusters* in the dendrites of pyramidal neurons,

28

610   are fundamental for guiding the rules for sensory perception, affecting the STDP learning rule,

611   learning and memory, and ultimately cognition.

612 **METHODS**

613 *Brain slice preparation and electrophysiology*. Brains from postnatal day 14-21 C57B/6 mice -

614 anesthetized with isoflurane - were removed and immersed in cold (4°C) oxygenated sucrose

615 cutting solution containing (in mM) 27 $NaHCO_3$, 1.5 NaH_2PO_4, 222 Sucrose, 2.6 KCl, 1 $CaCl_2$,

616 and 3 $MgSO_4$. Coronal brain slices (300-μm-thick) of visual cortex were prepared as described

617 [23]. Brain slices were incubated for 1/2 hour at 32°C in artificial cerebrospinal fluid (ACSF, in

618 mM: 126 NaCl, 26 $NaHCO_3$, 10 Dextrose, 1.15 NaH_2PO_4, 3 KCl, 2 $CaCl_2$, $2MgSO_4$) and then

619 transferred to a recording chamber. Electrophysiological recordings were performed in whole-

620 cell current-clamp configuration with MultiClamp 700B amplifiers (Molecular Devices) in L5

621 pyramidal neurons with a patch electrode (4-7 MΩ) filled with internal solution containing (in

622 mM) 0.1 Alexa Fluo 568, 130 Potassium D-Gluconic Acid (Potassium Gluconate), 2 $MgCl_2$, 5

623 KCl, 10 HEPES, 2 MgATP, 0.3 NaGTP, pH 7.4, and 0.4% Biocytin. All experiments were

624 conducted at room temperature (~20-22°C). We did not extend our experiments to include

625 voltage-clamp recordings since recent evidence indicates that the high spine neck resistance can

626 prevent the voltage-clamp control of excitatory synapses and that these measurements can be

627 significantly distorted in spiny neurons [66].

628

629 *Two-photon imaging and two-photon uncaging of glutamate*. Two-photon imaging was

630 performed with a custom-built two-photon laser scanning microscope, consisting of 1) a Prairie

631 scan head (Bruker) mounted on an Olympus BX51WI microscope with a 60X, 0.9 N.A. water

632 immersion objective; 2) a tunable Ti-Sapphire laser (Chameleon Ultra-II, Coherent, >3 W, 140-

633 fs pulses, 80 MHz repetition rate), 3) two photomultiplier tubes (PMT) for fluorescence

634 detection. Fluorescence images were detected with Prairie software (Bruker).

30

635   Fifteen minutes after break-in, two-photon scanning images of basal dendrites were obtained

636   with 720 nm and low power (~5 mW on sample (i.e., after the objective)) excitation light and

637   collected with a PMT. Two-photon uncaging of 4-methoxy-7-nitroindolinyl (MNI)-caged L-

638   glutamate (2.5 mM; Tocris) was performed as previously described [67]. This concentration of

639   MNI-glutamate completely blocked IPSCs [68], thus, our results represent excitatory inputs only.

640   Uncaging was performed at 720 nm (~25-30 mW on sample). Note that the laser power used for

641   imaging is not sufficient to result in any partial uncaging of glutamate (Fig. S9). Activated spines

642   were mostly on the second and third branch of the basal dendrites and were on average 40.22 ±

643   1.62 μm away from the soma (range of distances: ~10 to 80 μm from soma, n = 104 spines, Fig.

644   S10). Only spines with a clear head contour and that were separated by >1 μm from neighboring

645   spines were selected. The location of the uncaging spot was positioned at ~ 0.3 μm away from

646   the upper edge of the selected spine head (red dot in figures), which has a spatial resolution of

647   0.71 and 0.88 μm for one and two spines respectively (Fig. S11). Care was taken to maintain the

648   position of the uncaging spot. After each uncaging sequence, the spot was repositioned to keep

649   the same distance of ~ 0.3 μm from the edge of the soma and to avoid artificial potentiation or

650   depression. The uncaging-induced excitatory postsynaptic potentials (uEPSP) were recorded at

651   the soma of L5 pyramidal neurons. Importantly, the kinetics of uEPSPs from the present study

652   are not significantly different (10/90 rate of rise: 0.07 ± 0.014 mV/ms, p=0.92; duration: 115.5 ±

653   15.3 ms, p=0.65) from those triggered at 37°C [23].

654

655   *Spike-timing-dependent plasticity (STDP) induction protocol*: To induce t-LTP in single spines,

656   we used two-photon uncaging of MNI-glutamate (40 times every 2 seconds, with each uncaging

657   pulse lasting 2 ms), which, after 7 or 13 ms, was followed by a backpropagating action potential

658   (bAP) (triggered by a brief (10 ms) current injection (0.4 -0.6 nA) in the soma). To induce t-LTD

659   in single spines, two-photon uncaging of MNI-glutamate (40 times every 2 seconds, with each

660   uncaging pulse lasting 2 ms) was preceded for -15 or -23 ms by bAP. When we evaluated t-LTP

661   and t-LTD in two spines, we used similar protocols to those described above, but the spines were

662   activated with two-photon uncaging of MNI-glutamate sequentially with an onset delay of ~2.1

663   ms for the second spine. No significant difference was observed in the in 10/90 rise time of the

664   uEPSPs triggered when one versus two spines were activated (9.05 ± 1.19 ms versus 9.49 ± 0.54

665   ms, respectively; $p = 0.71$).

666   To evaluate the morphological and synaptic strength of the activated spines before and after the

667   STDP induction protocol, we performed 2P imaging, and low frequency 2P uncaging (0.5 Hz) in

668   single or multiple spines. To establish the time course of the changes in uEPSP amplitude, neck

669   length and head volume following STDP induction, for each experiment, we interpolated the

670   data taken at different time points using the *interp1* function in MATLAB (MathWorks) with the

671   *pchip* option, which performs a shape-preserving piecewise cubic interpolation. Note that we

672   constrained this fit so that it terminated with a slope of zero following the last data point. Then,

673   for each condition, we averaged the uEPSP amplitude, neck length and head volume temporal

674   traces. The length of the x-axis was set as the time at which the last data point was obtained for

675   those sets of experiments. Shaded area represents $\pm$SE. To determine at which time the uEPSP

676   amplitude, neck length and head volume temporal traces are significantly different from baseline,

677   we binned the temporal traces every 5min and tested whether it was significantly different from

678   baseline (100%).

32

679 The time at which the maximal change in uEPSP was observed after t-LTP and t-LTD induction

680 was used to calculate the percent change from control, and the percent changes in neck length

681 and head volume. These analyses are displayed in Figures 1 to 5.

682

683 *Experimental checkpoints and data analysis*: Electrophysiological data were analyzed with

684 Wavemetrics software (Igor Pro) and MATLAB. The resting membrane potential of the recorded

685 L5 pyramidal neurons was -60.25 ± 0.54 mV (recorded from a random sample of n = 58 neurons

686 from a total of n= 99 neurons tested), which is similar to what others have reported in acute

687 mouse brain slices of a similar age [69]. After taking this measurement, pyramidal neurons were

688 maintained at − 65 mV in current clamp configuration throughout the recording session. Only

689 neurons for which the injected current to hold the cell at − 65 mV was < 100 pA were included in

690 this study. For the generation of bAP, only action potentials (AP) with amplitude of > 45 mV

691 from threshold to the peak amplitude were considered for analysis. We found a mean AP

692 amplitude from threshold of 63.14 ± 1.73 mV before STDP induction which was similar to that

693 measured during the STDP protocol (63.17 ± 1.76 mV) and at all time points after the STDP

694 protocol (62.08 ± 1.91, pooled data of AP amplitude measured at all time points from each

695 experiment, p = 0.93; n = 58). No significant difference was found by comparing AP amplitude

696 before and after the STPD protocol (p > 0.5, paired t-test, n=58). The absolute AP amplitude,

697 measured from the membrane potential to the peak depolarization amplitude, before the STDP

698 protocol was 79.47 ± 2.21 mV (n = 58), and remained stable after the STDP protocol (80.11 ±

699 1.4 mV, pooled from all times after STDP, p = 0.93).

700 In most experiments, two control tests (each consisting of 10 uncaging pulses at 0.5 Hz), spaced

701 by 5 min were performed to assess the reliability of the uEPSP amplitude. Only experiments for

702 which uEPSP amplitudes were not significantly different before and after 5 minutes in control

703 conditions were considered for analysis (less than 10% variation).

704 Synaptic plasticity was assessed by two parameters: the uEPSP amplitude and the spine

705 morphology (neck length and head volume). The peak uEPSP amplitude was measured from

706 each individual uEPSP by taking the peak value and averaging 2 ms before and after using

707 Wavemetrics (Igor Pro). Only uEPSPs that were > 0.1 mV when one spine was activated in the

708 control condition (i.e., before the induction of plasticity) were included in the analysis.

709 Synaptic plasticity was determined by the relative change of uEPSP amplitude (average of 10

710 uEPSP) measured before and after the STDP protocol. For each experiment, we evaluated

711 whether the STDP protocol generated potentiation or depression by determining how many

712 uEPSP data points fell above or below baseline values over the course of the experiment.

713 Potentiation was defined as the majority of uEPSP amplitude data points measured over time

714 increasing relative to baseline, and the maximum uEPSP increase was used for statistical test.

715 Similar results were obtained when we instead considered the average uEPSP change following

716 STDP induction for each experiment. Depression was defined as the majority of uEPSP

717 amplitude data points measured over time decreasing relative to baseline, and the maximum

718 uEPSP decrease was used for statistical test. Similar results were obtained when we instead

719 considered the average uEPSP change following STDP induction for each experiment. The spike

720 timings +7 ms and +13 ms (pre leads post) or -23 ms and -15 ms (post leads pre) correspond to

721 the delta time offset between the beginning of the uncaging pulse (pre) and the beginning of the

722 bAP pulse (post) repeated 40 times.

723 The analysis of spine morphology was performed from z-projections of the whole spine using

724 ImageJ [70] (neck length) and MATLAB (MathWorks) (head volume). The neck length was

34

725 measured from the bottom edge of the spine head to the edge of its parent dendritic shaft using

726 the segmented line tool in ImageJ. We selected mostly spines with a spine neck longer than 0.2

727 µm. For those with a shorter neck, we did not report their length for analysis and statistics due to

728 the diffraction limited resolution of our images. For spines whose necks shrunk after the STDP

729 protocol below the diffraction limited resolution of our microscope, we set their length as the

730 minimal measurement of spine neck length reported by Tonnesen et al., using STED microscopy

731 (0.157 µm) [17]. We estimated the relative spine head volume using the ratio of the maximum

732 spine fluorescence and the maximum fluorescence observed in the dendrite measured from z-

733 projections of the whole spine [71, 72]. To obtain the spine volume, we then multiplied this ratio by

734 the PSF of our microscope (0.11 fL) [73]. Linear optimization techniques were used to determine

735 the correlation between EPSP change, neck length change and distance between 2 activated

736 spines. Specifically, the change in uEPSP amplitude was modeled using the following equation:

$$uEPSP = c_1 \times NL + c_2 \times D \qquad\qquad Equation\ 1$$

738 Where *uEPSP* and *NL* are the percent change in uEPSP and neck length, respectively, following

739 the STDP protocol, *D* is the distance between the 2 spines, and c_1, c_2 and c_3 are constant

740 coefficients. These parameters were estimated using a least squares technique to obtain an

741 optimal fit of the data that minimized the sum of the residuals squared. The relationship between

742 inter-spine distance and the percent change in uEPSP was fit with the following exponential

743 equation:

$$y = \alpha e^{\frac{-x}{\lambda}} + \beta \qquad\qquad Equation\ 2$$

745 where α, β and λ are constants, y represents the change in uEPSP, and x is the inter-spine

746 distance.

747

748   *Calcium imaging:* During calcium imaging experiments, we performed whole-cell current-clamp

749   recordings of L5 pyramidal neurons with a patch electrode containing calcium indicator Fluo-4

750   (300 μM; Thermo Fisher) and Alexa-594 (100 μM) diluted in an internal solution containing (in

751   mM) 130 D-Gluconic Acid, 2 $MgCl_2$, 5 KCl, 10 HEPES, 2 MgATP, 0.3 NaGTP, pH 7.4, and

752   0.4% Biocytin. To perform sequential 2P calcium imaging and 2P uncaging of caged glutamate

753   in selected spines at one wavelength (810 nm), we used ruthenium-bipyridine-

754   trimethylphosphine caged glutamate (RuBi-glu, Tocris) [68], diluted into the bath solution for a

755   final concentration of 800 μM. Uncaging of Rubi-glu was performed at 810 nm (~25-30 mW on

756   sample). The location of the uncaging spot was positioned at ~ 0.3 μm away from the upper edge

757   of the selected spine head (red dot in Figures 6-8). Changes in calcium were monitored by

758   imaging 2P calcium signals and detecting the fluorescence with 2 PMTs placed after wavelength

759   filters (525/70 for green, 595/50 for red). We performed 2P calcium imaging during five

760   different STDP induction protocols triggered at 0.5Hz: (1) pre-post pairing of +7 ms in one

761   spine; (2) pre-post pairing of +7 ms in two clustered spines; (3) pre-post pairing of +13 ms in one

762   spine; (4) post-pre pairing of -15 ms in one spine; (5) post-pre pairing of -15 ms in two clustered

763   spines. We restricted the image acquisition to a small area (~150 x 150 pixels) which contained

764   the spine(s) that we uncaged and the shaft. Images were acquired at ~ 30 Hz, averaged 8 times,

765   with 8 μs dwell time. Calcium signals were imaged 500 ms before STDP induction protocol and

766   right after (4ms) the stimulation for more than 600 ms. We focused our analysis on the images

767   obtained before and immediately after the stimulation in each pairing repetition. ROI drawing

768   was performed using custom algorithms (MATLAB; MathWorks). For spine heads, the ROI was

769   a circle whereas for dendrites it was a polygon. Fluorescence was computed as the mean of all

36

770 pixels within the ROI. We quantified the relative change in calcium concentration ($\frac{\Delta G}{R}$) using the

771 following formula:

772 $$\frac{\Delta G}{R} = \frac{G - G_{baseline}}{R} \qquad\qquad\qquad \textit{Equation 3}$$

773 where G is the fluorescence from the Fluo-4 dye and R is the fluorescence from the Alexa-594

774 dye. $G_{baseline}$ is the mean of all pixels of Fluo-4 signal within the ROI taken from the first image

775 at the first stimulation.

776

777 *Statistical analysis*: Statistics were performed with GraphPad Prism 5. Statistical significance

778 was determined using two-tailed Student's paired *t*-test when we analyzed the maximum change

779 in uEPSP amplitude after the induction of t-LTP or t-LTD in each experiment and the

780 concomitant changes in the activated spine morphology. Statistical significance was determined

781 using one-way repeated measures ANOVA when we analyzed the time course of the uEPSP

782 amplitude and spine morphological changes after induction of t-LTP or t-LTD with post-hoc

783 pairwise comparisons using Dunnett's test. *$P<0.05$; **$P<0.01$; ***$P<0.001$.

784

785 *Pharmacology*: Latrunculin A (Lat-A, Tocris Bioscience) was dissolved in DMSO at 1/1000 and

786 added to the recording chamber containing the brain slice at 100 nM for 15 min before starting

787 the STDP protocol. PEP1-TGL (Tocris Bioscience) was added in the pipette at 200 µM; after 15

788 min in whole cell condition, electrophysiological recording and synaptic plasticity experiments

789 were started. MNI-glutamate (Tocris Bioscience) was diluted in ACSF from stock solution and

790 bath applied at 2.5 mM. Fresh vials of MNI-glutamate were used for each experiment.

791

792 **Ethics**

37

793   *Animal experimentation*: these studies were performed in compliance with experimental

794   protocols (13-185, 15-002, 16-011 and 17-012) approved by the *Comité de déontologie de*

795   *l'expérimentation sur les animaux* (CDEA) of the University of Montreal.

796 **ACKNOWLEDGEMENTS**

807

808 **AUTHOR CONTRIBUTIONS**

809 R.A. conceived the project. S.T. and D.E.M. performed the experiments. S.T. and D.E.M.

810 performed data analyses. S.M-R. performed control experiments. R.A., S.T., and D.E.M.

811 designed experiments. R.A., S.T., and D.E.M. wrote the manuscript. R.A. supervised the project.

812 All authors read and approved the contents of the manuscript.

813

814 **DECLARATION OF INTEREST**

815 The authors declare no competing interests.

REFERENCES

1. Araya R. Input transformation by dendritic spines of pyramidal neurons. *Frontiers in neuroanatomy* **8**, (2014).

2. Araya R, Vogels TP, Yuste R. Activity-dependent dendritic spine neck changes are correlated with synaptic strength. *Proceedings of the National Academy of Sciences of the United States of America*, (2014).

3. Matsuzaki M, Ellis-Davies GCR, Nemoto T, Miyashita Y, Iino M, Kasai H. Dendritic spine geometry is critical for AMPA receptor expression in hippocampal CA1 pyramidal neurons. *Nature neuroscience* **4**, 1086-1092 (2001).

4. Matsuzaki M, Honkura N, Ellis-Davies GCR, Kasai H. Structural basis of long-term potentiation in single dendritic spines. *Nature* **429**, 761-766 (2004).

5. Harvey CD, Yasuda R, Zhong HN, Svoboda K. The spread of Ras activity triggered by activation of a single dendritic spine. *Science* **321**, 136-140 (2008).

6. Nishiyama J, Yasuda R. Biochemical Computation for Spine Structural Plasticity. *Neuron* **87**, 63-75 (2015).

7. Harvey CD, Svoboda K. Locally dynamic synaptic learning rules in pyramidal neuron dendrites. *Nature* **450**, 1195-1200 (2007).

8. Oh WC, Hill TC, Zito K. Synapse-specific and size-dependent mechanisms of spine structural plasticity accompanying synaptic weakening. *Proceedings of the National Academy of Sciences of the United States of America* **110**, E305-312 (2013).

9. Hayashi-Takagi A*, et al.* Labelling and optical erasure of synaptic memory traces in the motor cortex. *Nature* **525**, 333-+ (2015).

10. Feldman DE. The Spike-Timing Dependence of Plasticity. *Neuron* **75**, 556-571 (2012).

11. Bi GQ, Poo MM. Synaptic modifications in cultured hippocampal neurons: dependence on spike timing, synaptic strength, and postsynaptic cell type. *The Journal of neuroscience : the official journal of the Society for Neuroscience* **18**, 10464-10472 (1998).

12. Zhang LI, Tao HW, Holt CE, Harris WA, Poo MM. A critical window for cooperation and competition among developing retinotectal synapses. *Nature* **395**, 37-44 (1998).

13. Sjostrom PJ, Turrigiano GG, Nelson SB. Rate, timing, and cooperativity jointly determine cortical synaptic plasticity. *Neuron* **32**, 1149-1164 (2001).

14. Sjostrom PJ, Hausser M. A cooperative switch determines the sign of synaptic plasticity in distal dendrites of neocortical pyramidal neurons. *Neuron* **51**, 227-238 (2006).

15. Froemke RC, Poo MM, Dan Y. Spike-timing-dependent synaptic plasticity depends on dendritic location. *Nature* **434**, 221-225 (2005).

16. Froemke RC, Letzkus JJ, Kampa BM, Hang GB, Stuart GJ. Dendritic synapse location and neocortical spike-timing-dependent plasticity. *Frontiers in synaptic neuroscience* **2**, 29 (2010).

17. Tonnesen J, Katona G, Rozsa B, Nagerl UV. Spine neck plasticity regulates compartmentalization of synapses. *Nature neuroscience* **17**, 678-685 (2014).

18. Feldman DE. Timing-based LTP and LTD at vertical inputs to layer II/III pyramidal cells in rat barrel cortex. *Neuron* **27**, 45-56 (2000).

19. Nakamura T, Barbara JG, Nakamura K, Ross WN. Synergistic release of Ca2+ from IP3-sensitive stores evoked by synaptic activation of mGluRs paired with backpropagating action potentials. *Neuron* **24**, 727-737 (1999).

20. Hashimotodani Y*, et al.* Phospholipase Cbeta serves as a coincidence detector through its Ca2+ dependency for triggering retrograde endocannabinoid signal. *Neuron* **45**, 257-268 (2005).

21. Bender VA, Bender KJ, Brasier DJ, Feldman DE. Two coincidence detectors for spike timing-dependent plasticity in somatosensory cortex. *The Journal of neuroscience : the official journal of the Society for Neuroscience* **26**, 4166-4177 (2006).

22. Sjostrom PJ, Turrigiano GG, Nelson SB. Neocortical LTD via coincident activation of presynaptic NMDA and cannabinoid receptors. *Neuron* **39**, 641-654 (2003).

23. Araya R, Jiang J, Eisenthal KB, Yuste R. The spine neck filters membrane potentials. *Proceedings of the National Academy of Sciences of the United States of America* **103**, 17961-17966 (2006).

24. Richardson RJ, Blundon JA, Bayazitov IT, Zakharenko SS. Connectivity patterns revealed by mapping of active inputs on dendrites of thalamorecipient neurons in the auditory cortex. *The Journal of neuroscience : the official journal of the Society for Neuroscience* **29**, 6406-6417 (2009).

25. Harnett MT, Makara JK, Spruston N, Kath WL, Magee JC. Synaptic amplification by dendritic spines enhances input cooperativity. *Nature* **491**, 599-602 (2012).

26. Jayant K*, et al.* Targeted intracellular voltage recordings from dendritic spines using quantum-dot-coated nanopipettes. *Nature nanotechnology* **12**, 335-342 (2017).

41

27. Hayashi Y, Shi SH, Esteban JA, Piccini A, Poncer JC, Malinow R. Driving AMPA receptors into synapses by LTP and CaMKII: requirement for GluR1 and PDZ domain interaction. *Science* **287**, 2262-2267 (2000).

28. Ashby MC, Maier SR, Nishimune A, Henley JM. Lateral diffusion drives constitutive exchange of AMPA receptors at dendritic spines and is regulated by spine morphology. *The Journal of neuroscience : the official journal of the Society for Neuroscience* **26**, 7046-7055 (2006).

29. Holcman D, Triller A. Modeling synaptic dynamics driven by receptor lateral diffusion. *Biophysical journal* **91**, 2405-2415 (2006).

30. Kusters R, Kapitein LC, Hoogenraad CC, Storm C. Shape-induced asymmetric diffusion in dendritic spines allows efficient synaptic AMPA receptor trapping. *Biophysical journal* **105**, 2743-2750 (2013).

31. Holcman D, Schuss Z. Diffusion laws in dendritic spines. *Journal of mathematical neuroscience* **1**, 10 (2011).

32. Shim SH*, et al.* Super-resolution fluorescence imaging of organelles in live cells with photoswitchable membrane probes. *Proceedings of the National Academy of Sciences of the United States of America* **109**, 13978-13983 (2012).

33. Frost NA, Shroff H, Kong HH, Betzig E, Blanpied TA. Single-Molecule Discrimination of Discrete Perisynaptic and Distributed Sites of Actin Filament Assembly within Dendritic Spines. *Neuron* **67**, 86-99 (2010).

34. Allison DW, Gelfand VI, Spector I, Craig AM. Role of actin in anchoring postsynaptic receptors in cultured hippocampal neurons: Differential attachment of NMDA versus AMPA receptors. *Journal of Neuroscience* **18**, 2423-2436 (1998).

35. Hanley JG. Actin-dependent mechanisms in AMPA receptor trafficking. *Front Cell Neurosci* **8**, (2014).

36. Kim CH, Lisman JE. A role of actin filament in synaptic transmission and long-term potentiation. *Journal of Neuroscience* **19**, 4314-4324 (1999).

37. Honkura N, Matsuzaki M, Noguchi J, Ellis-Davies GCR, Kasai H. The subspine organization of actin fibers regulates the structure and plasticity of dendritic spines. *Neuron* **57**, 719-729 (2008).

38. Ramachandran B, Frey JU. Interfering with the actin network and its effect on long-term potentiation and synaptic tagging in hippocampal CA1 neurons in slices in vitro. *The Journal of neuroscience : the official journal of the Society for Neuroscience* **29**, 12167-12173 (2009).

953   39.   Lynch G, Larson J, Kelso S, Barrionuevo G, Schottler F. Intracellular injections of EGTA
954   block induction of hippocampal long-term potentiation. *Nature* **305**, 719-721 (1983).
955

956   40.   Malenka RC, Kauer JA, Zucker RS, Nicoll RA. Postsynaptic calcium is sufficient for
957   potentiation of hippocampal synaptic transmission. *Science* **242**, 81-84 (1988).
958

959   41.   Artola A, Singer W. Long-term depression of excitatory synaptic transmission and its
960   relationship to long-term potentiation. *Trends Neurosci* **16**, 480-487 (1993).
961

962   42.   Cummings JA, Mulkey RM, Nicoll RA, Malenka RC. Ca2+ signaling requirements for
963   long-term depression in the hippocampus. *Neuron* **16**, 825-833 (1996).
964

965   43.   Fino E, Paille V, Cui Y, Morera-Herreras T, Deniau JM, Venance L. Distinct coincidence
966   detectors govern the corticostriatal spike timing-dependent plasticity. *The Journal of*
967   *physiology* **588**, 3045-3062 (2010).
968

969   44.   Lisman J. A mechanism for the Hebb and the anti-Hebb processes underlying learning
970   and memory. *Proceedings of the National Academy of Sciences of the United States of*
971   *America* **86**, 9574-9578 (1989).
972

973   45.   Ismailov I, Kalikulov D, Inoue T, Friedlander MJ. The kinetic profile of intracellular
974   calcium predicts long-term potentiation and long-term depression. *The Journal of*
975   *neuroscience : the official journal of the Society for Neuroscience* **24**, 9847-9861 (2004).
976

977   46.   Nevian T, Sakmann B. Spine Ca2+ signaling in spike-timing-dependent plasticity.
978   *Journal of Neuroscience* **26**, 11001-11013 (2006).
979

980   47.   Graupner M, Brunel N. Mechanisms of induction and maintenance of spike-timing
981   dependent plasticity in biophysical synapse models. *Frontiers in computational*
982   *neuroscience* **4**, (2010).
983

984   48.   Rubin JE, Gerkin RC, Bi GQ, Chow CC. Calcium time course as a signal for spike-
985   timing-dependent plasticity. *J Neurophysiol* **93**, 2600-2613 (2005).
986

987   49.   Penn AC*, et al.* Hippocampal LTP and contextual learning require surface diffusion of
988   AMPA receptors. *Nature* **549**, 384-388 (2017).
989

990   50.   Tanaka JI, Horiike Y, Matsuzaki M, Miyazaki T, Ellis-Davies GCR, Kasai H. Protein
991   synthesis and neurotrophin-dependent structural plasticity of single dendritic spines.
992   *Science* **319**, 1683-1687 (2008).
993

994   51.   El-Boustani S*, et al.* Locally coordinated synaptic plasticity of visual cortex neurons in
995   vivo. *Science* **360**, 1349-1354 (2018).
996

52. Nevian T, Larkum ME, Polsky A, Schiller J. Properties of basal dendrites of layer 5 pyramidal neurons: a direct patch-clamp recording study. *Nature neuroscience* **10**, 206-214 (2007).

53. Markram H, Lubke J, Frotscher M, Roth A, Sakmann B. Physiology and anatomy of synaptic connections between thick tufted pyramidal neurones in the developing rat neocortex. *J Physiol-London* **500**, 409-440 (1997).

54. Schmidt H, Gour A, Straehle J, Boergens KM, Brecht M, Helmstaedter M. Axonal synapse sorting in medial entorhinal cortex. *Nature* **549**, 469-475 (2017).

55. Kasthuri N*, et al.* Saturated Reconstruction of a Volume of Neocortex. *Cell* **162**, 648-661 (2015).

56. Bloss EB, Cembrowski MS, Karsh B, Colonell J, Fetter RD, Spruston N. Single excitatory axons form clustered synapses onto CA1 pyramidal cell dendrites. *Nature neuroscience* **21**, 353-363 (2018).

57. Yang SN, Tang YG, Zucker RS. Selective induction of LTP and LTD by postsynaptic [Ca2+]i elevation. *J Neurophysiol* **81**, 781-787 (1999).

58. Karmarkar UR, Buonomano DV. A model of spike-timing dependent plasticity: one or two coincidence detectors? *J Neurophysiol* **88**, 507-513 (2002).

59. Shouval HZ, Bear MF, Cooper LN. A unified model of NMDA receptor-dependent bidirectional synaptic plasticity. *Proceedings of the National Academy of Sciences of the United States of America* **99**, 10831-10836 (2002).

60. Schiemann J*, et al.* Cellular mechanisms underlying behavioral state-dependent bidirectional modulation of motor cortex output. *Cell Rep* **11**, 1319-1330 (2015).

61. Wilson DE, Whitney DE, Scholl B, Fitzpatrick D. Orientation selectivity and the functional clustering of synaptic inputs in primary visual cortex. *Nature neuroscience* **19**, 1003-1009 (2016).

62. Scholl B, Wilson, D.E., Fitzpatrick, D. Local Order within Global Disorder: Synaptic Architecture of Visual Space. In: *Neuron* (ed^(eds) (2017).

63. Lee WC*, et al.* Anatomy and function of an excitatory network in the visual cortex. *Nature* **532**, 370-374 (2016).

64. Lee KS, Vandemark K, Mezey D, Shultz N, Fitzpatrick D. Functional Synaptic Architecture of Callosal Inputs in Mouse Primary Visual Cortex. *Neuron*, (2019).

65. Lee KF, Soares C, Thivierge JP, Beique JC. Correlated Synaptic Inputs Drive Dendritic Calcium Amplification and Cooperative Plasticity during Clustered Synapse Development. *Neuron* **89**, 784-799 (2016).

66. Beaulieu-Laroche L, Harnett MT. Dendritic Spines Prevent Synaptic Voltage Clamp. *Neuron* **97**, 75-82 e73 (2018).

67. Araya R, Eisenthal KB, Yuste R. Dendritic spines linearize the summation of excitatory potentials. *Proceedings of the National Academy of Sciences of the United States of America* **103**, 18799-18804 (2006).

68. Fino E, Araya R, Peterka DS, Salierno M, Etchenique R, Yuste R. RuBi-Glutamate: Two-Photon and Visible-Light Photoactivation of Neurons and Dendritic spines. *Frontiers in neural circuits* **3**, 2 (2009).

69. Le Bon-Jego M, Yuste R. Persistently active, pacemaker-like neurons in neocortex. *Frontiers in neuroscience* **1**, 123-129 (2007).

70. Rasband WS, Bright DS. Nih Image - a Public Domain Image-Processing Program for the Macintosh. *Microbeam Anal* **4**, 137-149 (1995).

71. Nimchinsky EA, Yasuda R, Oertner TG, Svoboda K. The number of glutamate receptors opened by synaptic stimulation in single hippocampal spines. *The Journal of neuroscience : the official journal of the Society for Neuroscience* **24**, 2054-2064 (2004).

72. Holtmaat AJ*, et al.* Transient and persistent dendritic spines in the neocortex in vivo. *Neuron* **45**, 279-291 (2005).

73. Ruttinger S, Buschmann V, Kramer B, Erdmann R, Macdonald R, Koberling F. Comparison and accuracy of methods to determine the confocal volume for quantitative fluorescence correlation spectroscopy. *J Microsc* **232**, 343-352 (2008).
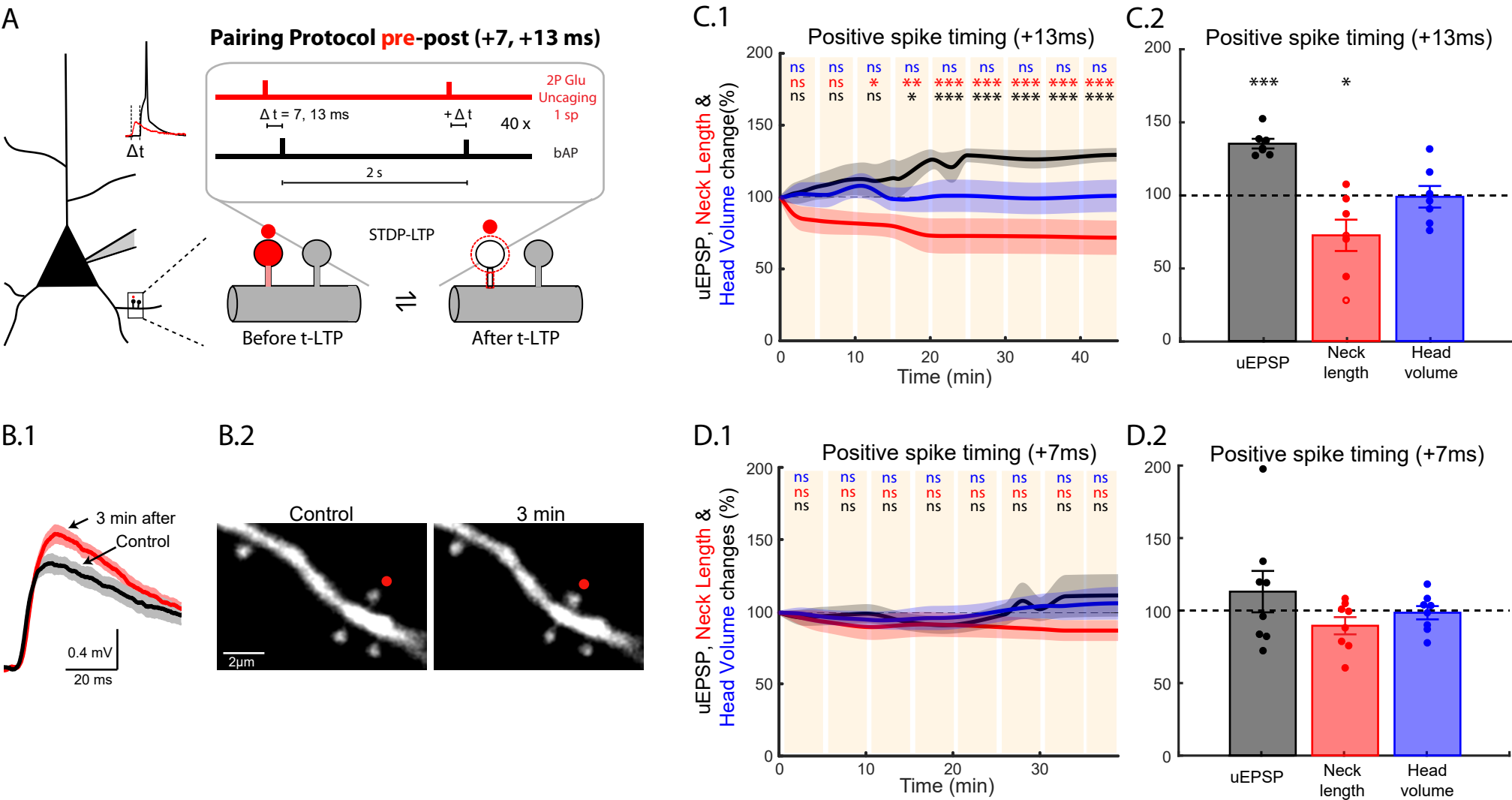
Figure 1

1074 **Figure 1**: **Induction of t-LTP in single dendritic spines**. (A) Experimental protocol for the

1075 induction of t-LTP with pre-post pairings (two-photon (2P) uncaging of glutamate followed by a

1076 bAP) of +7 and +13 ms in single dendritic spines (sp). (B) Example of a t-LTP protocol with pre-

1077 post pairing protocol of + 13 ms. (B.1) Average uEPSP response recorded via a whole-cell

1078 pipette at the soma of L5 pyramidal neurons before (Control) and after the induction of t-LTP in

1079 a selected dendritic spine located in basal dendrites (B.2). Traces in B.1 correspond to an average

1080 of 10 depolarizations generated by 2P uncaging over the indicated spine (B.2 red dot) before

1081 (black trace) and after the induction of t-LTP (red trace). (C.1) Time course of uEPSP amplitude

1082 (black line), neck length (red line) and spine head volume (blue line) changes over the course of

1083 40 min following STDP induction in individual spines at a pre-post timing of + 13 ms. *ns*, not

1084 significant; *P < 0.05; **P < 0.01; ***P < 0.001, one-way repeated measures ANOVA followed

1085 by post hoc Dunnet's test. (C.2) Maximum changes in uEPSP amplitude (black bar and dots) and

1086 concomitant changes in neck length (red bar and dots) and head volume (blue bar and dots) of

1087 the activated spine after the induction of t-LTP at a pre-post timing of +13 ms. *P < 0.05, ***P <

1088 0.001, paired t-test. (D.1) Time course of uEPSP amplitude (black line), neck length (red line)

1089 and spine head volume (blue line) changes over the course of ~40 min following STDP induction

1090 in individual spines at a pre-post timing of + 7 ms. *ns*, not significant; *P < 0.05, one-way

1091 repeated measures ANOVA followed by post hoc Dunnet's test. (D.2) Maximum changes in

1092 uEPSP amplitude (black bar and dots) and corresponding changes in neck length (red bar and

1093 dots) and head volume (blue bar and dots) of the activated spine after the induction of t-LTP at a

1094 pre-post timing of +7 ms. Shaded light area in C.1 and D.1, and error bars in C.2 and D.2

1095 represent ±SEM. Time 0 in C.1 and D.1 is the time when the 40 pre-post repetitions of the

1096 induction protocol were completed.

1097

46

Figure 2

A — Pairing Protocol post-pre (-15, -23 ms); Δt = -15, -23 ms; 2P Glu Uncaging 1 sp; 40 x; bAP; 2 s; -Δt; STDP-LTD; Before t-LTD; After t-LTD

B.1 — Control; 15 min after; 0.2 mV; 20 ms

B.2 — Control; 15 min; 2μm

C.1 — Negative spike timing (-15ms)

C.2 — Negative spike timing (-15ms)

D.1 — Negative spike timing (-23ms)

D.2 — Negative spike timing (-23ms)
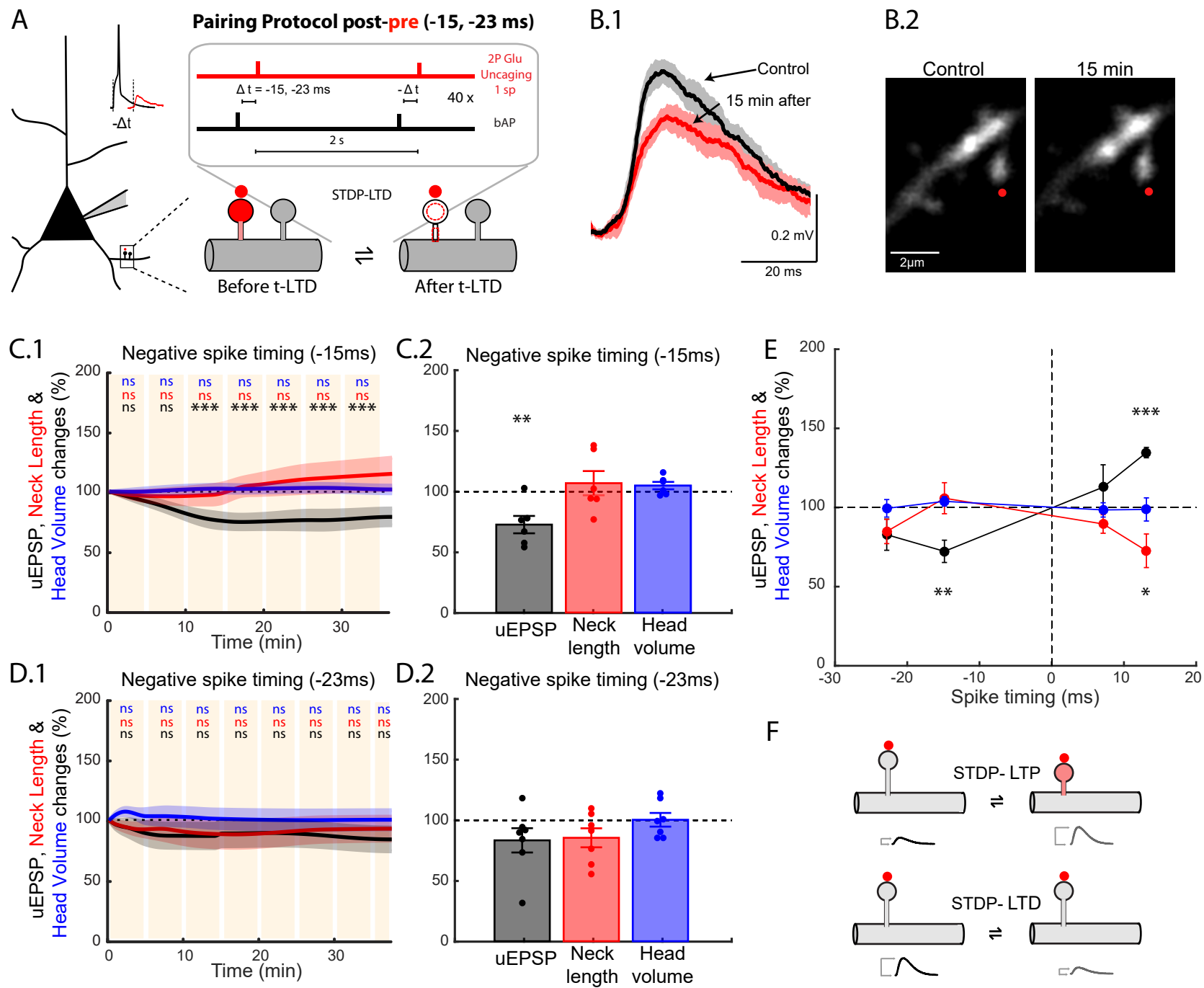
E

F — STDP- LTP; STDP- LTD

1098 **Figure 2**: **Induction of t-LTD in single dendritic spines**. (A) Experimental protocol for the

1099 induction of t-LTD with post-pre pairings protocols of -15 and -23 ms in single dendritic spines.

1100 (B) Example of a t-LTD protocol with post-pre pairings protocol of -15 ms. (B.1) Average

1101 uEPSP response recorded via a whole-cell pipette at the soma of L5 pyramidal neurons before

1102 (Control) and after the induction of t-LTD in selected dendritic spines located in basal dendrites

1103 (B.2). Traces in B.1 correspond to an average of 10 uEPSP generated by the 2P uncaging of

1104 glutamate at the indicated spine (B.2, red dot) before (black trace) and after the induction of t-

1105 LTD (red trace). (C.1) Time course of uEPSP amplitude (black line), neck length (red line) and

1106 spine head volume (blue line) changes over the course of ~35 min following STDP induction in

1107 individual spines at a post-pre timing of -15 ms. *ns*, not significant; ***P < 0.001, one-way

1108 repeated measures ANOVA followed by post hoc Dunnet's test. (C.2) Maximum changes in

1109 uEPSP amplitude (black bar and dots) and concomitant changes in neck length (red bar and dots)

1110 and head size of the activated spine (blue bar and dots) after the induction of t-LTD at a post-pre

1111 timing of -15 ms. **P < 0.01, paired t test. (D.1) Time course of uEPSP amplitude (black line),

1112 neck length (red line) and spine head volume (blue line) changes over the course of ~ 40 min

1113 following STDP induction in individual spines at a post-pre timing of -23 ms. *ns*, not significant,

1114 one-way repeated measures ANOVA followed by post hoc Dunnet's test. (D.2) Maximum

1115 changes in uEPSP amplitude (black bar and dots) and corresponding changes in neck length (red

1116 bar and dots) and head volume (blue bar and dots) of the activated spine after the induction of t-

1117 LTD at a post-pre timing of -23 ms. Shaded light area in C.1 and D.1, and error bars in C.2 and

1118 D.2 represent ±SEM. Time 0 in C.1 and D.1 is the time when the 40 pre-post repetitions of the

1119 induction protocol were completed. (E) STDP learning rule for single dendritic spines: Plot

1120 illustrating the maximum changes in uEPSP amplitude (black data points), and concomitant

47

1121   changes in neck length (red data points) and head volume (blue data points) after the induction of

1122   t-LTP (temporal offset +13 ms and +7 ms) and t-LTD (temporal offset -15 ms and -23 ms). *P <

1123   0.05, **P < 0.01, paired t test. (F) Diagram indicating the uEPSP amplitude and spine neck

1124   morphological changes observed after the induction of t-LTP and t-LTD.
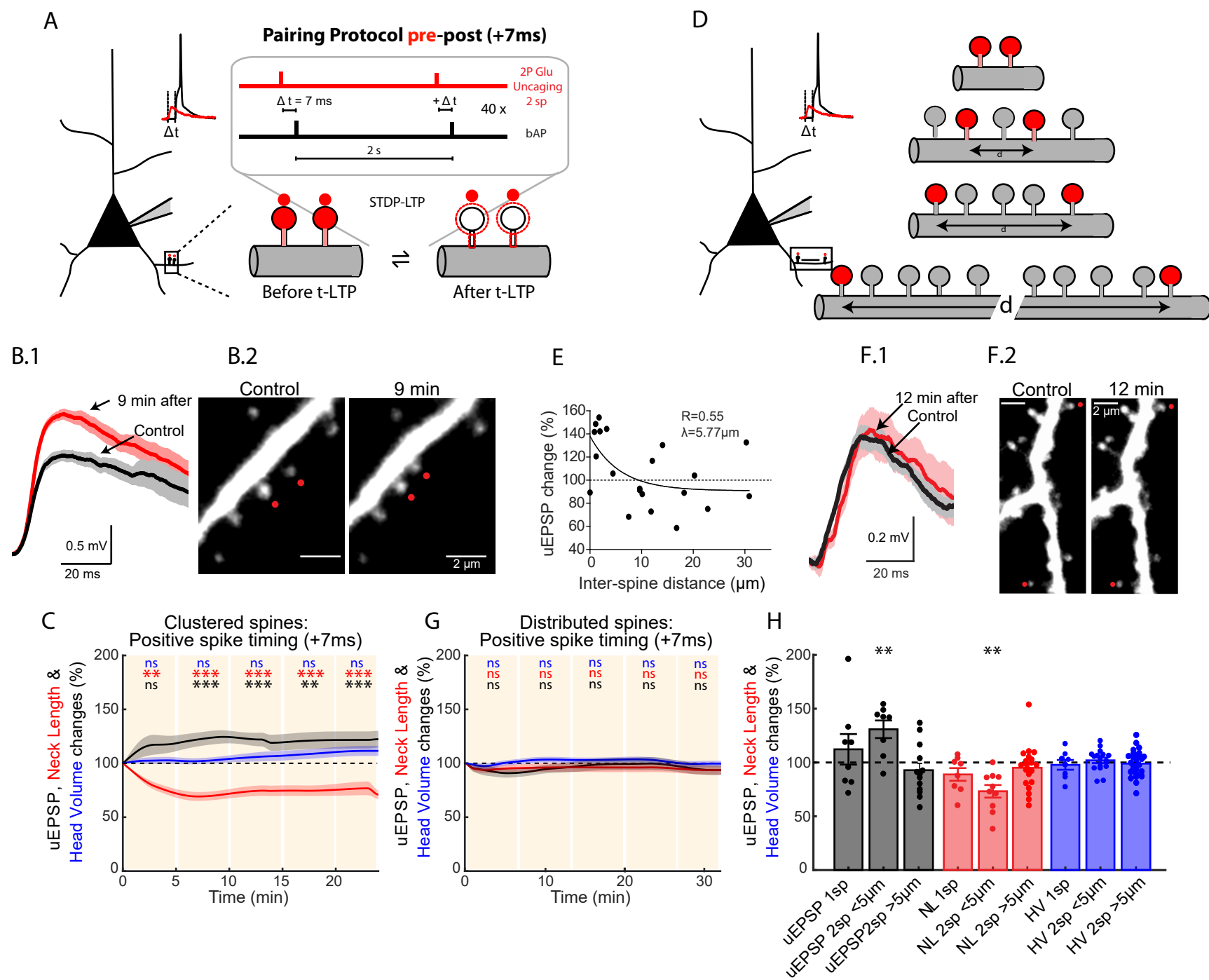
Figure 3

1125 **Figure 3**: **Induction of t-LTP in clustered and distributed dendritic spines** (A) Experimental

1126 protocol for the induction of t-LTP (pre-post timing of + 7 ms) in two clustered dendritic spines

1127 (< 5 μm distance between spines). (B) Example of one experiment where two neighbouring

1128 dendritic spines were activated with a pre-post t-LTP protocol. (B.1) Average uEPSP response

1129 recorded via a whole-cell pipette at the soma of L5 pyramidal neurons before (Control) and after

1130 the induction of t-LTP in two selected dendritic spines located in a basal dendrite (red dots, B.2).

1131 Traces in B.1 correspond to an average of 10 uEPSP generated by the 2P uncaging at the

1132 indicated spines (B.2) before (black trace) and after the induction of t-LTP (red trace). (C) Time

1133 course of uEPSP amplitude (black line), neck length (red line) and spine head volume (blue line)

1134 changes over the course of ~25 min following STDP induction in clustered spines (< 5μm

1135 distance between spines) at a pre-post timing of + 7 ms. *ns*, not significant; **P < 0.01, ***P <

1136 0.001, one-way repeated measures ANOVA followed by post hoc Dunnet's test. (D)

1137 Experimental protocol for the induction of t-LTP (pre-post timing of + 7 ms) in two distributed

1138 spines (> 5μm distance between spines). (E) Induction of t-LTP (increase in uEPSP amplitude,

1139 more than 100%) in two nearly simultaneously activated spines at a pre-post timing of + 7 ms is

1140 dependent on inter-spine distance. Data points represent mean. We use the extracted value of λ as

1141 a boundary between clustered and distributed spines. (F) Example of one experiment where two

1142 distributed dendritic spines (> 5μm distance between spines) were activated with a pre-post

1143 timing of + 7ms. (F.1) Average uEPSP response recorded via a whole-cell pipette at the soma of

1144 L5 pyramidal neurons before (Control) and after the induction of t-LTP in two selected dendritic

1145 spines located in a basal dendrite (red dots, F.2). Traces in F.1 correspond to an average of 10

1146 uEPSP generated by the 2P uncaging at the indicated spines (F.2) before (black trace) and after

1147 the induction of t-LTP (red trace). (G) Time course of uEPSP amplitude (black line), neck length

49

1148   (red line) and spine head volume (blue line) changes over the course of ~30 min following STDP

1149   induction in distributed spines (> 5μm distance between spines) at a pre-post timing of + 7 ms.

1150   *ns*, not significant; **P < 0.01, ***P < 0.001, one-way repeated measures ANOVA followed by

1151   post hoc Dunnet's test. (H) Pooled data of the maximum changes in uEPSP amplitude (black bar

1152   and dots) and concomitant changes in neck length (red bar and dots) and head volume (blue bar

1153   and dots) of individual (1sp), clustered (< 5μm) and distributed (> 5μm) spines (2sp) after the

1154   induction of t-LTP at a pre-post timing of +7ms. **P < 0.01, paired t test. Shaded light area in

1155   B.1, F.1C and G and error bars in H represent ±SEM. Time 0 in C and G is the time when the 40

1156   pre-post repetitions of the induction protocol are completed. NL = neck length, HV = head
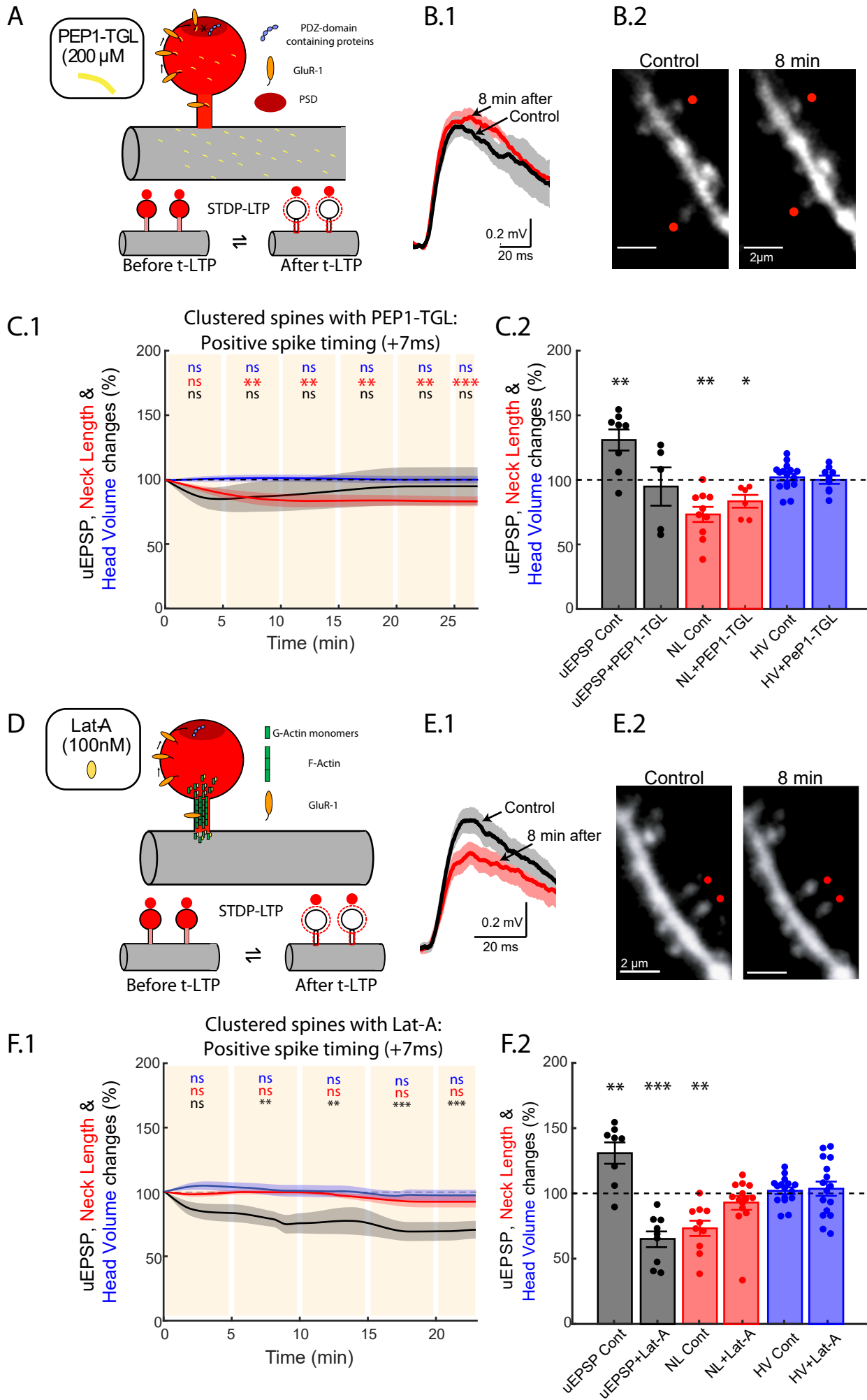
1157   volume.

Figure 4

1158 **Figure 4**: **Molecular mechanisms responsible for the induction of t-LTP**. (A) Experimental

1159 protocol for the induction of t-LTP (pre-post timing of + 7 ms) in two clustered dendritic spines

1160 (< 5 μm) in the presence of PEP1-TGL (200 μM). (B) An example of one experiment where two

1161 neighbouring dendritic spines were activated with a pre-post t-LTP protocol in the presence of

1162 PEP1-TGL. (B.1) Average uEPSP recorded via a whole-cell pipette at the soma of L5 pyramidal

1163 neurons before (Control) and after the induction of t-LTP in two selected dendritic spines located

1164 in basal dendrites (B.2). Traces in B.1 correspond to an average of 10 uEPSP generated by the 2P

1165 uncaging of glutamate at the two indicated spines (red dots, B.2) before (black trace) and after

1166 the induction of t-LTP in the presence of PEP1-TGL (red traces). (C.1) Time course of uEPSP

1167 amplitude (black line), neck length (red line) and spine head volume (blue line) changes over the

1168 course of ~28 min following STDP induction in clustered spines at a pre-post timing of + 7 ms in

1169 the presence of PEP1-TGL. *ns*, not significant; **P < 0.01, ***P < 0.001, one-way repeated

1170 measures ANOVA followed by post hoc Dunnet's test. (C.2) Pooled data of the maximum

1171 changes in uEPSP amplitude (black bar and dots) and concomitant changes in neck length (red

1172 bar and dots) and head volume (blue bar and dots) of the activated clustered spines after the

1173 induction of t-LTP at a pre-post timing of +7ms in control conditions (Cont) and in the presence

1174 of PEP1-TGL (PEP1-TGL). *P < 0.05, **P < 0.01, paired t test. Time 0 is the time when the 40

1175 pre-post repetitions of the induction protocol were completed. (D) Experimental protocol for the

1176 induction of t-LTP (pre-post timing of + 7 ms) in two clustered dendritic spines (< 30μm) in the

1177 presence Latrunculin-A (Lat-A, 100nM). (E) Example of one experiment where two

1178 neighbouring dendritic spines were activated with a pre-post t-LTP protocol in the presence of

1179 Lat-A. (E.1) Average uEPSP recorded via a whole-cell pipette at the soma of L5 pyramidal

1180 neurons before (Control) and after the induction of t-LTP in two selected dendritic spines (red

1181   dots, E.2) located in basal dendrites (E.2). Traces in E.1 correspond to an average of 10 uEPSP

1182   generated by the 2P uncaging over the two indicated spines (red dots, E.2) before (black trace)

1183   and after the induction of t-LTP in the presence of Lat-A (red trace). (F.1) Time course of uEPSP

1184   amplitude (black line), neck length (red line) and spine head volume (blue line) changes over the

1185   course of ~12 min following STDP induction in clustered spines at a pre-post timing of + 7 ms in

1186   the presence of Lat-A. *ns*, not significant; **P < 0.01, ***P < 0.001, one-way repeated measures

1187   ANOVA followed by post hoc Dunnet's test. (F.2) Pooled data of the maximum changes in

1188   uEPSP amplitude (black bar and dots) and concomitant changes in neck length (red bar and dots)

1189   and head volume (blue bar and dots) of the activated clustered spines after the induction of t-LTP

1190   at a pre-post timing of +7 ms in control conditions (Cont) and in the presence of Lat-A (Lat-A).

1191   **P < 0.01, ***P < 0.001, paired t test. NL = neck length, HV = head volume. Shaded light area

1192   in C.1 and F.1 and error bars in C.2 and F.2 represent ±SEM. Time 0 is the time when 40 pre-

1193   post repetitions of the induction protocol were completed.
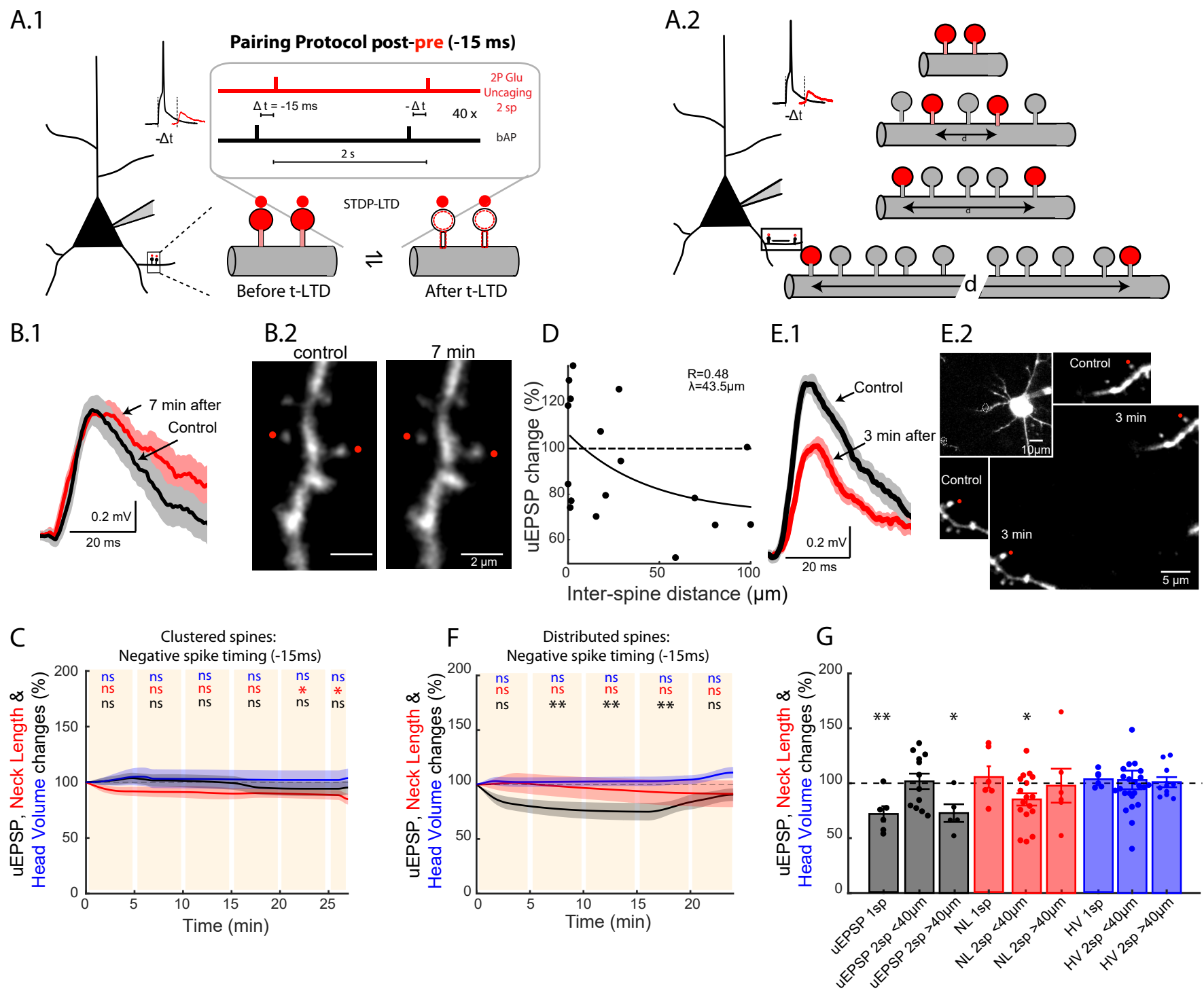
52

Figure 5

1194   **Figure 5. Induction of t-LTD in clustered and distributed dendritic spines:** (A) Experimental

1195   protocol for the induction of t-LTD protocol (pairings of - 15 ms) in two clustered dendritic

1196   spines (< 40 µm) (A.1), or in two distributed spines (> 40 µm distance between spines). (B) An

1197   example of one experiment where two neighbouring dendritic spines were activated with a post-

1198   pre t-LTP protocol of -15 ms. (B.1) Average uEPSP recorded via a whole-cell pipette at the

1199   soma of L5 pyramidal neurons before (Control) and after the induction of t-LTD in two selected

1200   dendritic spines (red dots, B.2) located in basal dendrites. Traces in B.1 correspond to an average

1201   of 10 uEPSP generated by 2P uncaging of glutamate at the indicated spines before (black trace)

1202   and after the induction of t-LTD (red trace). (C) Time course of uEPSP amplitude (black line),

1203   the neck length (red line) and spine head volume (blue line) of the activated clustered spines after

1204   the induction of t-LTD at pairings of -15 ms. *ns*, not significant; *P < 0.05, one-way repeated

1205   measures ANOVA followed by post hoc Dunnet's test. (D) t-LTD recovery (decrease in uEPSP

1206   amplitude, less than 100%) is dependent on inter-spine distance. Each data point represents the

1207   maximal change in uEPSP from each experiment. We use the extracted value of λ as a boundary

1208   between clustered and distributed spines. (F) Example of one experiment where two distributed

1209   dendritic spines (> 40 µm distance between spines) were activated with a post-pre timing -15 ms.

1210   (F.1) Average uEPSP response recorded via a whole-cell pipette at the soma of L5 pyramidal

1211   neurons before (Control, underneath image, F.2) and 3 min after the induction of t-LTD (F.2,

1212   over imposed image) in two selected dendritic spines located in basal dendrites. (F.2) Inset

1213   shows a low magnification image of the recorded neuron with the marked location of the

1214   selected spines. Traces in F.1 correspond to an average of 10 uEPSP generated by 2P uncaging at

1215   the indicated spines (red dots, F.2) before (black trace) and after the induction of t-LTD (red

1216   trace). (G) Time course of uEPSP amplitude (black line), the neck length (red line) and spine

53

1217   head volume (blue line) of the activated distributed spines (> 40 μm) after the induction of t-

1218   LTD at pairings of -15 ms. *ns*, not significant; *P < 0.05, **P < 0.01, one-way repeated measures

1219   ANOVA followed by post hoc Dunnet's test.   (H) Pooled data of the maximum changes in

1220   uEPSP amplitude (black bar and dots) and concomitant changes in neck length (red bar and dots)

1221   and head volume (blue bar and dots) of individual (1sp), clustered (2sp at < 40 μm) and

1222   distributed spines (2sp at > 40 μm) after the induction of t-LTD at a post-pre timing of -15 ms.

1223   *P < 0.05, **P < 0.01, paired t test.   Time 0 in C and G is the time when the 40 pre-post

1224   repetitions of the induction protocol were completed. NL = neck length, HV = head volume.
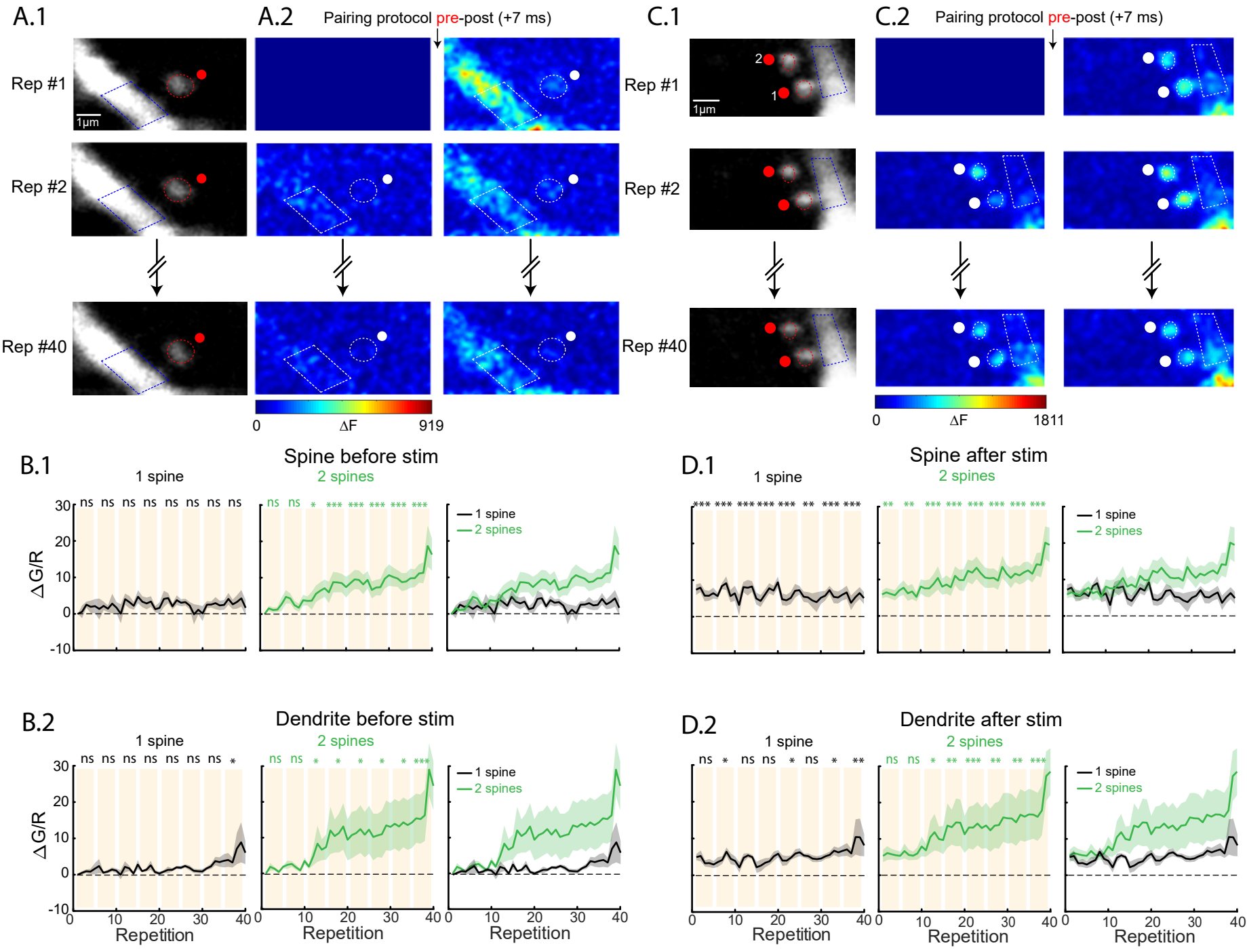
Figure 6

A.1

Rep #1   Rep #2   Rep #40

1µm

A.2   Pairing protocol pre-post (+7 ms)

ΔF   0   919

C.1

Rep #1   Rep #2   Rep #40

1µm

C.2   Pairing protocol pre-post (+7 ms)

ΔF   0   1811

B.1   Spine before stim
1 spine   2 spines

ΔG/R

Repetition

B.2   Dendrite before stim
1 spine   2 spines

ΔG/R

Repetition

D.1   Spine after stim
1 spine   2 spines

Repetition

D.2   Dendrite after stim
1 spine   2 spines

Repetition

1225 **Figure 6. Calcium dynamics in single and two clustered spines during a pre-post pairing**

1226 **protocol of + 7ms.** (A.1) Single 2P images of a spine and dendrite from a L5 pyramidal neuron

1227 loaded with Alexa 594 (100uM) and Fluo4 (300uM). Red ellipses and blue polygons indicate the

1228 ROIs selected for the calcium signal analysis. (A.2) Two photon calcium signal images before

1229 (left panels) and after (right panels) a pre-post pairing protocol (+7 ms). The 1st, 2nd, and 40th

1230 repetitions of the pairing protocol are shown here. The change in calcium fluorescence from

1231 baseline (ΔF) is color coded. Only positive changes in fluorescence are shown. (B) Population

1232 averages of the calcium signals ($\frac{\Delta G}{R}$) measured in spines (B.1) and dendrites (B.2) before the

1233 pairing protocol performed in 1 spine (left panels) and 2 spines (middle panels). The right panels

1234 shows the superimposed $\frac{\Delta G}{R}$ population averages in 1 spine (black lines) and 2 spines (green

1235 lines). (C.1) Single 2P images of two clustered spines and dendrite from a L5 pyramidal neuron

1236 loaded with Alexa 594 (100μM) and Fluo4 (300μM). Red ellipses and blue polygons indicate the

1237 ROIs selected for the calcium signal analysis. (C.2) Two photon calcium signal images before

1238 (left panel) and after (right panels) a pre-post pairing protocol (+ 7ms). The 1st, 2nd, and 40th

1239 repetitions of the pairing protocol are shown here. The change in calcium fluorescence from

1240 baseline (ΔF) is color coded. Only positive changes in fluorescence are shown. (D) Population

1241 averages of the calcium signals ($\frac{\Delta G}{R}$) measured in spines (D.1) and dendrites (D.2) after the

1242 pairing protocol performed in one spine (left panels) and two spines (middle panels). The right

1243 panels shows the superimposed $\frac{\Delta G}{R}$ population averages in one spine (black lines) and two spines

1244 (green lines). *ns*, not significant; *P < 0.05; **P < 0.01; ***P < 0.001, one-way repeated

1245 measures ANOVA followed by post hoc Dunnet's test.

1246

Figure 7

A.1

Rep #1

Rep #2

Rep #40

2 μm

A.2

Pairing protocol pre-post (+13 ms)

ΔF

25   623

B.1 Spine before stim

ΔG/R

** *** *** *** *** *** *** *** ***

15

10

5

0

B.2 Dendrite before stim

ΔG/R

** *** *** *** *** *** *** *** ***

15

10

5

0

0   10   20   30   40
Repetition

C.1 Spine after stim

*** *** *** *** *** *** *** *** ***

C.2 Dendrite after stim

*** *** *** *** *** *** *** *** ***

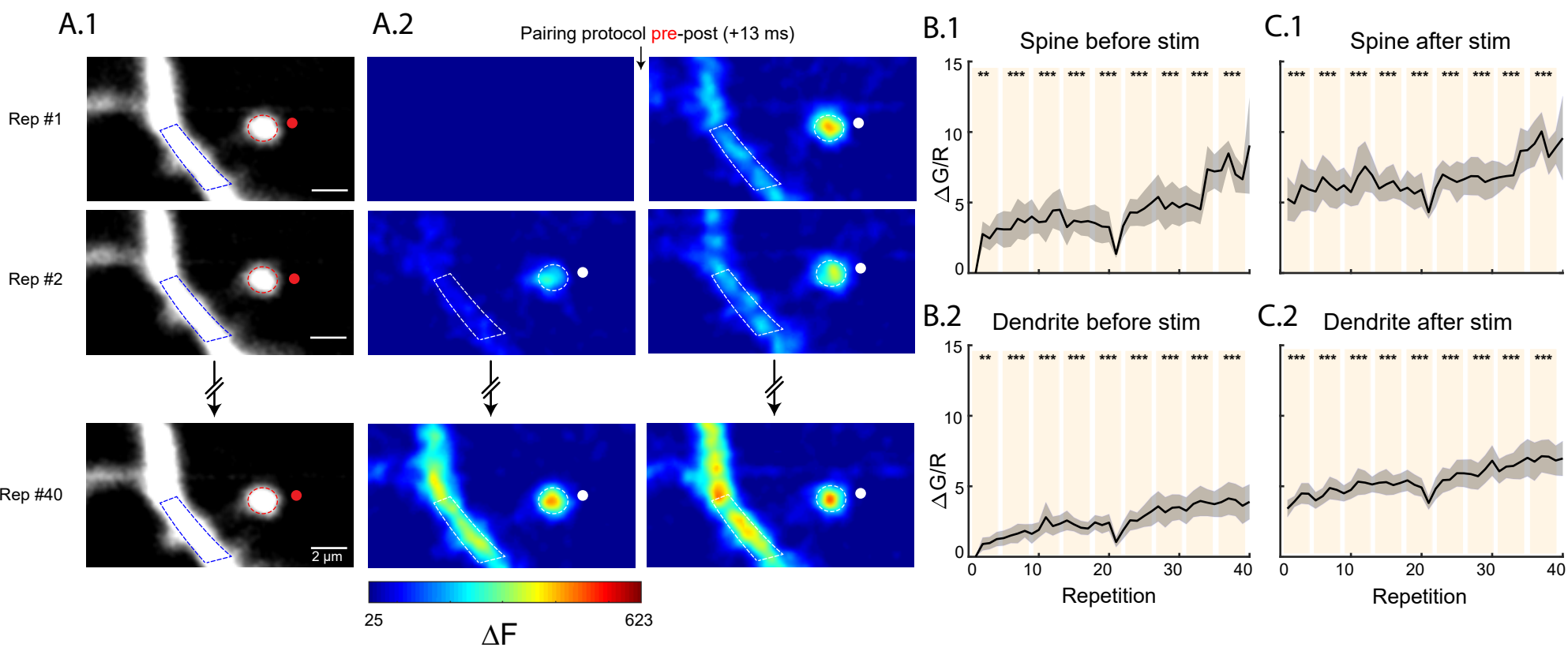0   10   20   30   40
Repetition

1247 **Figure 7. Calcium dynamics in single spines during a pre-post pairing protocol of +13ms.**

1248 (A.1) Single 2P images of a spine and dendrite from a L5 pyramidal neuron loaded with Alexa

1249 594 (100μM) and Fluo4 (300μM). Red ellipses and blue polygons indicate the ROIs selected for

1250 the calcium signal analysis. (A.2) Two photon calcium signal images before (left panels) and

1251 after (right panels) a pre-post pairing protocol of +13 ms. The 1st, 2nd, and 40th repetitions of the

1252 pairing protocol are shown here. The change in calcium fluorescence from baseline (ΔF) is color

1253 coded. Only positive changes in fluorescence are shown. (B) Population averages of the calcium

1254 signals ($\frac{\Delta G}{R}$) measured in spines (B.1 and C.1) and dendrites (B.2 and C.2) before (B) and after

1255 (C) the pairing protocol. *ns,* not significant; *P < 0.05; **P < 0.01; ***P < 0.001, one-way

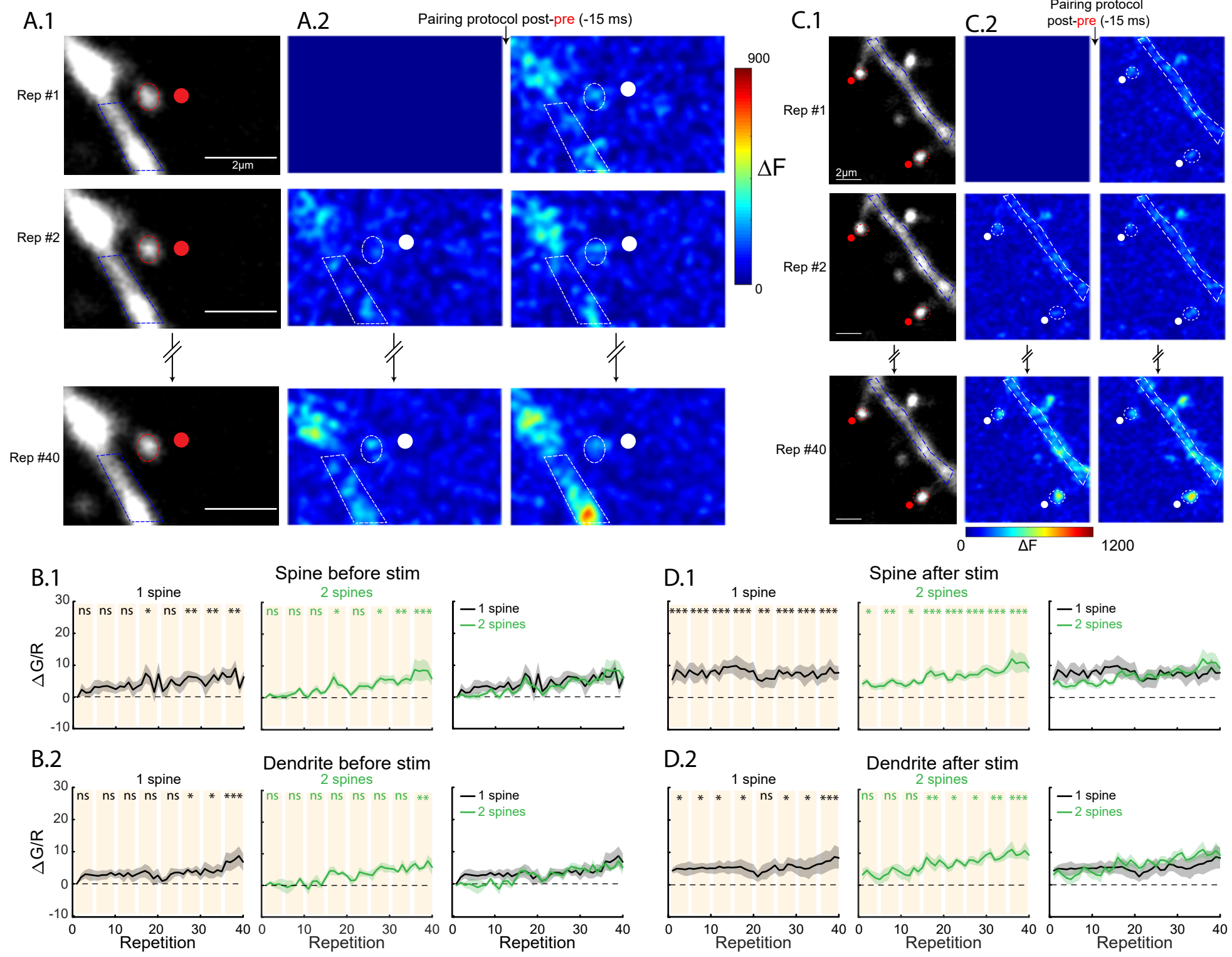1256 repeated measures ANOVA followed by post hoc Dunnet's test.

1257

Figure 8

1258 **Figure 8. Calcium dynamics in single and two clustered spines during post-pre pairing**

1259 **protocol.** (A1) Single 2P images of a spine and dendrite from a L5 pyramidal neuron loaded

1260 with Alexa 594 (100μM) and Fluo4 (300μM). Red ellipses and blue polygons indicate the ROIs

1261 selected for the calcium signal analysis. (A.2) Two photon calcium signal images before (left

1262 panels) and after (right panels) a post-pre pairing protocol (-15 ms). The 1st, 2nd, and 40th

1263 repetitions of the pairing protocol are shown here. The change in calcium fluorescence from

1264 baseline (ΔF) is color coded. Only positive changes in fluorescence are shown. (B) Population

1265 averages of the calcium signals ($\frac{\Delta G}{R}$) measured in spines (B.1) and dendrites (B.2) before the

1266 pairing protocol performed in one spine (left panels) and two spines (middle panels). The right

1267 panels shows the superimposed $\frac{\Delta G}{R}$ population averages in one spine (black lines) and two

1268 clustered spines (green lines). (C.1) Single 2P images of two clustered spines and dendrite from a

1269 L5 pyramidal neuron loaded with Alexa 594 (100μM) and Fluo4 (300μM). Red ellipses and blue

1270 polygons indicate the ROIs selected for the calcium signal analysis. (C.2) Two photon calcium

1271 signal images before (left panel) and after (right panels) a pre-post pairing protocol (-15 ms). The

1272 1st, 2nd, and 40th repetitions of the pairing protocol are shown here. The change in calcium

1273 fluorescence from baseline (ΔF) is color coded. Only positive changes in fluorescence are

1274 shown. (D) Population averages of the calcium signals ($\frac{\Delta G}{R}$) measured in spines (D.1) and

1275 dendrites (D.2) after the pairing protocol performed in one spine (left panels) and two spines

1276 (middle panels). The right panels shows the superimposed $\frac{\Delta G}{R}$ population averages in 1 spine

1277 (black lines) and 2 spines (green lines). *ns*, not significant; *P < 0.05; **P < 0.01; ***P < 0.001,

1278 one-way repeated measures ANOVA followed by post hoc Dunnet's test.
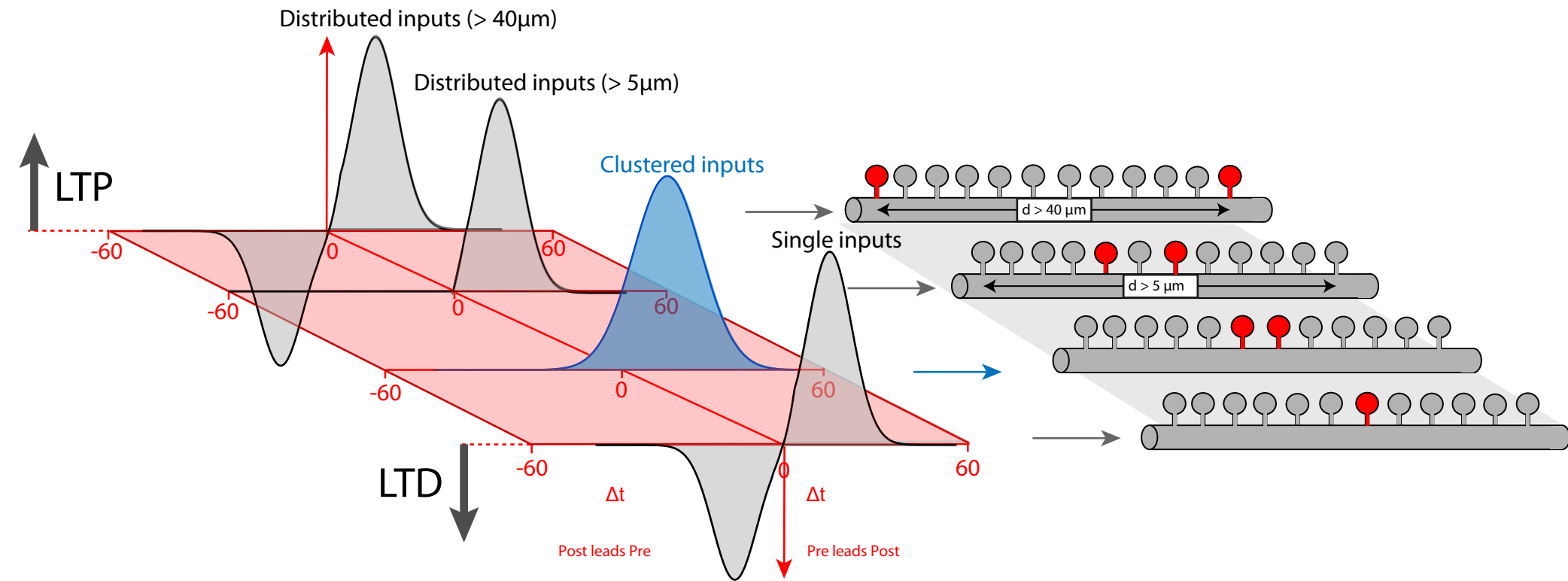
1279

Figure 9

1280 **Figure 9. STDP learning rule for single distributed and clustered dendritic spines.** STDP

1281 learning rule in the basal dendrites of L5 pyramidal neurons as a function of the structural

1282 organization of excitatory inputs in basal dendrites of L5 pyramidal neurons. Note how STDP in

1283 single, or distributed spines (separated by > 40 μm), follow a bidirectional Hebbian STDP rule.

1284 Importantly, our model indicate that the induction of t-LTD can be disrupted by the co-activation

1285 of two clustered spines separated by < 40 μm, and t-LTP enhanced by the co-activation of two

1286 clustered spines separated by < 40 μm by synaptic cooperativity. We propose that synaptic

1287 cooperativity generates local dendritic depolarization high enough to disrupt bidirectional STDP,

1288 leading to STDP that only encompasses LTP.

58